



HAL
open science

RAD50 promotes DNA repair by homologous recombination and restrains antigenic variation in African trypanosomes

Ann-Kathrin Mehnert, Marco Prorocic, Annick Dujeancourt-Henry, Sebastian Hutchinson, Richard Mcculloch, Lucy Glover

► To cite this version:

Ann-Kathrin Mehnert, Marco Prorocic, Annick Dujeancourt-Henry, Sebastian Hutchinson, Richard Mcculloch, et al.. RAD50 promotes DNA repair by homologous recombination and restrains antigenic variation in African trypanosomes. 2021. pasteur-03107143

HAL Id: pasteur-03107143

<https://pasteur.hal.science/pasteur-03107143>

Preprint submitted on 12 Jan 2021

HAL is a multi-disciplinary open access archive for the deposit and dissemination of scientific research documents, whether they are published or not. The documents may come from teaching and research institutions in France or abroad, or from public or private research centers.

L'archive ouverte pluridisciplinaire **HAL**, est destinée au dépôt et à la diffusion de documents scientifiques de niveau recherche, publiés ou non, émanant des établissements d'enseignement et de recherche français ou étrangers, des laboratoires publics ou privés.

Copyright

1 RAD50 promotes DNA repair by homologous recombination and 2 restrains antigenic variation in African trypanosomes

3

4 Ann-Kathrin Mehnert¹, Marco Prorocic², Annick Dujeancourt-Henry¹, Sebastian Hutchinson³, Richard
5 McCulloch², Lucy Glover^{1*}

6

7 ¹ Trypanosome Molecular Biology, Department of Parasites and Insect Vectors, Institut Pasteur, 25-28
8 Rue du Docteur Roux 75015, Paris, France.

9

10 ² Wellcome Center for Integrative Parasitology, Sir Graeme Davis Building, 120 University Place,
11 Glasgow, G12 8TA, UK.

12

13 ³ Trypanosome Cell Biology, Department of Parasites and Insect Vectors, Institut Pasteur, 25-28 Rue
14 du Docteur Roux 75015, Paris, France.

15

16 Present address: : Centre for Infectious Diseases, Virology, Heidelberg University Hospital, Im
17 Neuenheimer Feld 344, 69120 Heidelberg, Germany

18

19

20 * To whom correspondence should be addressed lucy.glover@pasteur.fr; Tel: +33 140613425

21

22 KEYWORDS: VSG, RAD50, DNA damage.

23 Abstract 147 words

24

25 **ABSTRACT**

26 Homologous recombination dominates as the major form of DNA repair in *Trypanosoma brucei*, and is
27 especially important for recombination of the subtelomeric variant surface glycoprotein during
28 antigenic variation. RAD50, a component of the MRN complex (MRE11, RAD50, NBS1), is central to
29 homologous recombination through facilitating resection and governing the DNA damage response.

30 The function of RAD50 in trypanosomes is untested. Here we report that RAD50 is required for
31 RAD51-dependent homologous recombination, phosphorylation of histone H2A and controlled
32 resection following a DNA double strand break (DSB). Perhaps surprisingly, DSB resection in the
33 *rad50* nulls was not impaired and appeared to peak earlier than in the parental strains. Finally, we
34 show that RAD50 suppresses DNA repair using donors with short stretches of homology at a
35 subtelomeric locus, with null strains producing a greater diversity of expressed VSG variants following
36 DSB repair. We conclude that RAD50 promotes stringent homologous recombination at subtelomeric
37 loci and restrains antigenic variation.

38

39 INTRODUCTION

40

41 *Trypanosoma brucei* (*T. brucei*) is a protozoan parasite and the causative agent of human African
42 trypanosomiasis, or sleeping sickness, and nagana in cattle. Trypanosomes cycle between their insect
43 vector, the tsetse fly, and mammalian hosts, where they colonise the blood, fat ¹ and skin ² and
44 eventually cross the blood brain barrier in late stage infection. If left untreated, trypanosomiasis is
45 normally fatal³. In the mammalian host, each trypanosome cell is covered in a dense layer of a single
46 species of variant surface glycoprotein (VSG). The highly immunogenic VSG layer^{4,5} acts as an
47 barrier, concealing other surface components from the host immune response ⁶. Trypanosomes
48 maintain a persistent infection by continuously escaping the host's immune response through antigenic
49 variation⁷. Central to this survival strategy is monoallelic expression of the VSG from a subtelomeric
50 locus, known as an expression site (VSG-ES), and stochastic VSG switching. The ~ 15 VSG-ESs in
51 the trypanosome genome share a high degree of sequence and structure conservation ⁸, each being
52 an RNA polymerase-I (RNA Pol-I) polycistronic transcription unit with a single VSG gene found
53 adjacent to the telomere, up to 60 kb downstream of the promoter ⁸. The VSG gene is flanked by two
54 sets of repetitive sequence: downstream is the telomere, and upstream is a block of repetitive
55 sequence, known as the 70-bp repeats, which modulates VSG switching ^{8,9}. Characteristic of a
56 trypanosome infection are recrudescence waves of parasitemia, each of which is composed of a diverse
57 VSG expressing population, with between 7 – 79 VSGs detected in each peak of parasitemia ¹⁰⁻¹².
58 VSG diversity arises through altering the single VSG-ES that is transcribed or, more commonly, by
59 recombination of silent VSGs into the active VSG-ES. The seemingly unrestricted use of VSG genes
60 might be expected to result in a rapid exhaustion of the VSG gene repertoire. However, the parasite's
61 ability to sustain an infection appears to lie in an enormous repertoire of >2000 VSG genes and
62 pseudogenes¹³⁻¹⁵, mainly found in subtelomeric VSG arrays, and a capacity for generation of novel
63 'mosaic' VSG genes through segmental gene conversion of multiple (pseudo) VSGs, in particular late
64 in infection ^{10,11,14}. Importantly, almost all of the array VSGs are associated with upstream tracts of 70-
65 bp repeats, providing the necessary substrate needed for homologous recombination mediated
66 antigenic variation ¹⁶.

67

68 A DNA double-strand break (DSB) is an extremely toxic lesion in any cell, which if left unrepaired can
69 lead to cell death. In *T. brucei* RAD51-dependent homologous recombination (HR) dominates as the
70 major DNA repair and recombination pathway, with microhomology mediated end-joining (MMEJ)
71 playing a minor role ¹⁷⁻²⁰. HR is important for VSG switching, and though it is not clear how MMEJ acts
72 in this reaction, repair of induced DSBs can occur by coupled HR and MMEJ, and MMEJ is more
73 frequently used for repair of DSBs induced within the VSG-ES²¹. Unrepaired DSBs appear to persist
74 throughout the cell cycle without inhibiting the trypanosomes ability to replicate their DNA²², but
75 whether HR or MMEJ are regulated is unknown. In addition, non-homologous end-joining (NHEJ)
76 appears to be absent in trypanosomes ^{21,23,24}. These features of trypanosome DSB repair contrast with
77 mammalian cells, where NHEJ is highly active, HR predominates in S and G₂ phase cells and MMEJ
78 is considered a minor reaction ²⁵. In trypanosomes both transcriptionally active and silent

79 subtelomeres are fragile ^{26,27}, and accumulate natural breaks. Within the active VSG-ES specifically, a
80 DSB between the VSG and 70-bp repeats acts as a potent driver of antigenic variation and
81 precipitates VSG switching ²⁷. Several DNA repair and recombination proteins have been shown to be
82 important for antigenic variation in trypanosomes, thus linking VSG switching with this process: loss of
83 RAD51 ¹⁸, the RAD51-3 paralogue ²⁸, or the RAD51-interacting protein BRCA2 ^{29,30} results in
84 impaired VSG switching, while loss of RECQ2 ³¹, TOPO3 α or RMI1 increases VSG switching ^{32,33}, as
85 does loss of the histone variants H3.V and H4.V ¹⁵. Loss of ATR, which is involved in DNA damage
86 signalling, impairs monoallelic VSG expression and increases VSG switching through localized DNA
87 damage ³⁴. Histone Acetyltransferase (HAT3) is required for recombination repair of a chromosome-
88 internal DSB, but suppresses DSB repair within the VSG-ES which suggests repair is
89 compartmentalised in trypanosomes ³⁵.

90
91 The DNA damage response (DDR) is an orchestrated cellular response to many different genome
92 lesions, including DSBs, which most commonly form via stalled replication forks ³⁶. Critical to DSB
93 repair is the MRE11 – RAD50 – NBS1 (MRN) complex (in yeast MRE11 – RAD50 – XRS1, MRX),
94 which acts as a DNA damage sensing complex and is responsible for recognizing the free DNA ends,
95 where it is one of the first complexes to bind and initiate HR ^{37,38}. MRE11 – RAD50 forms the core of
96 this complex and is conserved across all domains of life, whereas NBS1 only forms part of the
97 complex in eukaryotes ³⁷. MRN consists of two molecules of each component protein, and diffuses
98 along homoduplex DNA searching for free DNA ends – a process that is driven by RAD50 ³⁹. The
99 MRE11 subunit is a nuclease with both 5' flap endonuclease activity and 3'→5' exonuclease activity
100 and catalyses resection through cleaving the 5' strand, internal to the DSB, which is then resected
101 using its exonuclease function to generate the short 3' single-strand (ss) DNA overhangs ⁴⁰. These
102 overhangs are further resected by Exonuclease 1 (EXO1), forming long tracts of 3 ssDNA on either
103 side of the DSB ³⁹. NBS1, the eukaryote specific component, is responsible for binding multiple
104 phosphorylated proteins and recruiting MRE11 and RAD50 to DSB sites ⁴¹ through its interaction
105 with MRE11, CtIP, which is also required for initiating resection, and the ATM kinase ⁴². End
106 recognition and DSB processing by MRN is an ATP dependent process: here, ATP binding to
107 RAD50 acts to switch the complex from an open to a closed conformation ⁴³, which facilitates DSB
108 recognition, tethering and ATM activation ⁴³. In yeast the MRX complex also acts in telomere
109 maintenance by binding the end of short telomeres and recruiting TEL1, which then recruits
110 telomerase to extend the telomere ⁴⁴. Conversely, in mammalian cells, MRN regulates an ATM
111 dependent response at dysfunctional telomeres ⁴⁵.

112
113 RAD50 (Tb.927.11.8210), MRE11 (Tb927.2.4390) ^{46,47} and NBS1 (Tb 927.8.5710) homologues are
114 present in the trypanosome genome and previous studies have shown that MRE11 is required for HR
115 but its inactivation did not lead to telomere shortening or changes in VSG switching ^{46,47}, despite the
116 dominance of HR in repair in trypanosomes and requirement for the reaction in antigenic variation.
117 What roles these proteins play in the trypanosome DDR is largely unexplored. In addition, though we
118 know that DSBs accumulate at the subtelomeres ^{26,27}, it is unclear how they are sensed or how they

119 contribute to antigenic variation. Given the central, early role of the MRN complex in DSB recognition
120 and in telomere maintenance we set out to characterise its role in HR and VSG switching in
121 trypanosomes. We found that RAD50, like MRE11, is required for efficient HR, and in its absence
122 MMEJ dominated as the major form of repair. RAD50 also plays a perhaps surprising role in VSG
123 switching, where it restricts HR substrate selection in the VSG repertoire and so may act to preserve
124 the VSG archive during long-term infections.

125

126 **MATERIALS AND METHODS**

127 *Trypanosoma brucei* growth and manipulation. Lister 427, MITat1.2 (clone 221a), bloodstream stage
128 cells were cultured in HMI-11 medium ⁷⁹ at 37.4 °C with 5 % CO₂. Cell density was determined using a
129 haemocytometer. For transformation, 2.5 x 10⁷ cells were spun for 10 minutes at 1000g at room
130 temperature and the supernatant discarded. The cell pellet was resuspend in prewarmed cytomix
131 solution ⁸⁰ with 10 µg linearised DNA and place in a 0.2 cm gap cuvette, and nucleofected (Lonza)
132 using the X-001 program. The transfected cells were placed into one 25 cm² culture flask per
133 transfection with 36 ml warmed HMI-11 medium only and place in an incubator to allow the cells to
134 recover for approximately 6 hours. After 6 hours, the media distributed into 48-well plates with the
135 appropriate drug selection. Strains expressing TetR and I-SceI with I-SceI recognition-sites at a
136 chromosome-internal locus ¹⁷ and an active VSG-ESs ²⁷ have been described previously. G418, and
137 blasticidin were selected at 10 µg.ml⁻¹ and 2 µg.ml⁻¹ respectively. Puromycin, phleomycin, G418,
138 hygromycin and blasticidin and tetracycline were maintained at 1 µg.ml⁻¹. Clonogenic assay were
139 plated out at either 32 cells per plate under both inducing and non-inducing conditions for ¹HR and
140 VSG^{up} strains and 480 cells per plate for VSG^{up} strains under inducing conditions. Plates were
141 counted 5-6 days later and subclones selected for further analysis.

142 To generate the *RAD50* nulls in the ¹HR strain we employed multi-step transfection strategy ⁸¹
143 that recycled a *Neomycin phosphotransferase* gene (*NEO*) in order to rescue one marker (here
144 *Blasticidin* - *BLA*). Briefly, an I-SceI recognition sites was inserted into the pRAD50-BLA knock-out
145 cassette between the 5'UTR and *BLA* ORF (Figure 1C) in the 2T1 cell line ⁸² with a tetracycline
146 inducible *Sce* ORF. Induction of *Sce* induces a break in the *BLA* cassette and subsequent repair,
147 using homology in the *NEO* modified allele, replaces *BLA* with *NEO*.

148 Clonogenic assays were plated out at either 32 cells per plate under both inducing and non-
149 inducing conditions for ¹HR and VSG^{up} strains and 480 cells per plate for VSG^{up} strains under inducing
150 conditions. Plates were counted 5-6 days later and subclones selected for further analysis.

151

152 Plasmid construction. For native C-terminal epitope tagging of Tb927.5.1700 / *RPA2* a 765-bp
153 fragment was amplified using primers RPA28F:GATCAAGCTTATGGAAGGAAGTGAAGTAA; and
154 RPA28R:GATCTCTAGAAATGCCAACTTACAATCATG and cloned in pNAT^{xTAG} ⁸³ using the HindIII
155 and XbaI sites (underlined). The construct was linearized with XhoI prior to transfection. MRE11F5
156 (GATCgcgccgcATGGCCGAGAGGGCATC), MRE11R5 (GATCtctagaCAACGAAGATGTATGCCC),
157 MRE11F3 (GATCgggcccCGATGGATAGTGGTAAT) and

158 MRE11R3 (GATCggtaccCTAATAGTTATCTGGCA) were used to clone in target regions to generate
159 pMRE11KOBLA and pMRE11KONEO. For transfection, 20 µg pMRE11KO *Blasticidin* (BLA) and
160 *Neomycin* (NEO) plasmids were sequentially digested with Acc65I and NotI and cleaned by phenol-
161 chloroform extraction and ethanol precipitation after each digestion. Strains were validated using
162 MRE11F5 and MRE11R3 in a PCR assay. Heterozygous (+/-) and homozygous (-/-) knockout mutants
163 of *RAD50* were generated by deleting most of replacing most of the gene's open reading frame with
164 either BLA and NEO. The strategy used is as described in ⁸⁴; briefly, two modified versions of the
165 plasmid pmt123 were used to allow PCR-amplified 5' and 3' flanking untranslated regions of *RAD50* to
166 be inserted around BLA and NEO cassettes (where the antibiotic resistance genes' ORF were flanked
167 by tubulin and actin intergenic regions). The selective drug markers, flanked by *RAD50* 5' and 3'
168 untranslated regions, were then excised using NotI and transfected into *T. brucei*, and clones selected
169 using 10 µg.mL⁻¹ blasticidin or 5 µg.mL⁻¹ G418.

170
171 Immunofluorescence microscopy. Immunofluorescence analysis was carried out using standard
172 protocols as described previously ⁸⁵. Mouse α-Myc was used at 1:400 and rabbit α-γH2A ⁵⁵ was used
173 at 1:250. Fluorescein-conjugated goat α-rabbit and goat α-mouse secondary antibodies (Pierce) were
174 used at 1:2000. Samples were mounted in Vectashield (Vector Laboratories) containing 4, 6-
175 diamidino-2-phenylindole (DAPI). In *T. brucei*, DAPI-stained nuclear and mitochondrial DNA can be
176 used as cytological markers for cell cycle stage ⁸⁶; one nucleus and one kinetoplast (1N:1K) indicate
177 G₁, one nucleus and an elongated kinetoplast (1N:eK) indicate S phase, one nucleus and two
178 kinetoplasts (1N:2K) indicate G₂/M and two nuclei and two kinetoplasts (2N:2K) indicate post-mitosis.
179 Images were captured using a ZEISS Imager 72 epifluorescence microscope with an AxioCam 506
180 mono camera and images were processed and in ImageJ.

181
182 DNA analysis. Slot blots for detection of ssDNA were carried as described previously ¹⁷. ImageJ was
183 used to generate linear density plots. The VSG probe was a 750 bp fragment VSG2 fragment from a
184 Pst1 digest of pNEG. The *RFP* probe was a 687-bp HindIII/NotI fragment encompassing the full ORF.
185 Loading control was a 226 – bp product from *Tb427.01.570* (Dot1bKOF):
186 TGGTCGGAAGTTGGATGTGA Dot1bKOR: CTTCCATGCATAACACGCGA).

187
188 PCR analysis of *RAD50* nulls to confirms knock-out were done using standard PCR conditions with
189 the following primers; a 402 bp product for *RAD50* using RAD50KOF
190 (CGTGAGAAACAGGAACAGCA) and RAD50KOR (AACACGTTTTTCCAACCTCGG); a 399 bp product
191 for *Blasticidin* ORF using BlaF (GATCGAATTCATGGCCAAGCCTTTGTCT) and BlaR
192 (GATCCCATGGTTAGCCCTCCACACATAA); and a 795 bp product for *Neomycin*
193 *Phosphotransferase* ORF using NPTF (ATGATTGAACAAGATGGATTG) and NPTR
194 (TCAGAAGAACTCGTCAAGAA). Analysis of subclones was previously described^{21,27,35} and used the
195 following primers VSG221F (CTTCCAATCAGGAGGC), VSG221R (CGGCGACAACTGCAG), RFP
196 (ATGGTGCCTCCTCCAAGAAC), PAC (TCAGGCACCGGGCTTGC), ESAG1F

197 (AATGGAAGAGCAAAGCTGATAGGTTGG), ESAG1R (GGCGGCCACTCCATTGTCTG), 2110X
198 (GGGGTGAATGTTGGCTGTG), 2110Y (GGGATTCCCAGACCAATGA)

199

200 VSG sequencing analysis. For the RT-PCR, the reaction mix were as following; 1 µg of cDNA, 1 x
201 PCR buffer, 0.2 mM dNTPs, 1 µl each of SL (ACAGTTTCTGTACTATATTG) and SP6-14mer
202 (GATTTAGGTGACACTATAGTGTTAAAATATATC) primers, H₂O to 50 µl and 0.5 µl Phusion
203 polymerase (New England Biolabs). For the PCR conditions. Five cycles were carried out at 94 °C for
204 30s, 50 °C for 30s and 72 °C for 2 min; followed by 18 cycles at 94 °C for 30s, 55 °C for 30s and 72 °C
205 for 2 min. DNA concentration was measured using a Nanodrop. Libraries were prepared from VSG
206 PCR products and sequenced on a BGI-Seq (BGI500) with a 150 bp paired-end read length with BGI
207 Genomics Hong Kong.

208 Replicate libraries for WT uninduced, WT induced, VSG^{UP} uninduced and VSG^{UP} induced ,
209 VSG^{UP}*rad50* uninduced and VSG^{UP}*rad50* induced were sequenced on the BGISEQ500 platform
210 producing 8.03, 9.01, 7.60, 7.22, 6.66, 7.07, 6.90, 6.98 million reads per library, respectively. Reads
211 were aligned to the *T. brucei* Lister 427 genome¹⁵ with the cohort of minichromosomal VSGs added
212 from the Lister 427 VSGnome¹³ using bowtie2⁸⁷ with the parameters --very-sensitive and BAM files
213 created with samtools⁸⁸, aligning (WT uninduced) 97.76, 98.42, (WT induced) 97.69, (VSG^{UP}*rad50*
214 uninduced) 97.57, 98.60, (VSG^{UP}*rad50* induced) 97.63, 97.80 percent of reads successfully. Reads
215 counts per transcript were obtained using featureCounts⁸⁹. Differential expression analysis was
216 performed using EdgeR⁹⁰ on all genes, followed by filtering for VSG genes (1848 VSG sequences in
217 total). An R script (<https://github.com/LGloverTMB/DNA-repair-mutant-VSG-seq>) was used to perform
218 differential expression analysis, and generate Volcano and genome scale plots. BLAST analysis was
219 performed locally using a database containing significantly up-regulated VSG genes from both
220 conditions, including 2 kb of sequence upstream and downstream of the start and stop codons,
221 respectively (except where sequences in the contigs 5' or 3' to the CDS were shorter than 2 kb
222 excluding). For this analysis, minichromosomal VSG genes were excluded as the VSGnome does not
223 contain any sequence beyond the CDS. The resulting database of 131 VSGs was queried using the
224 VSG2 sequence including 2 kb of sequence upstream of the CDS and all sequence between the stop
225 codon and end of contig (1,272 nt). The BLASTn algorithm was used query the database using default
226 parameters except allowing up-to 20 hits per subject sequence, and outputting up to 2,000 alignments.
227 Alignments were filtered to remove overlapping hits from the same subject sequence using Microsoft
228 Excel, retaining the one with the higher alignment score. Non-overlapping alignments were plotted
229 using a custom R script (<https://github.com/LGloverTMB/DNA-repair-mutant-VSG-seq>). Lengths of
230 average alignments were calculated for cohorts of VSGs up-regulated in both VSG^{UP} and VSG^{UP}*rad50*
231 or VSG^{UP}*rad50* only.

232

233 RESULTS

234

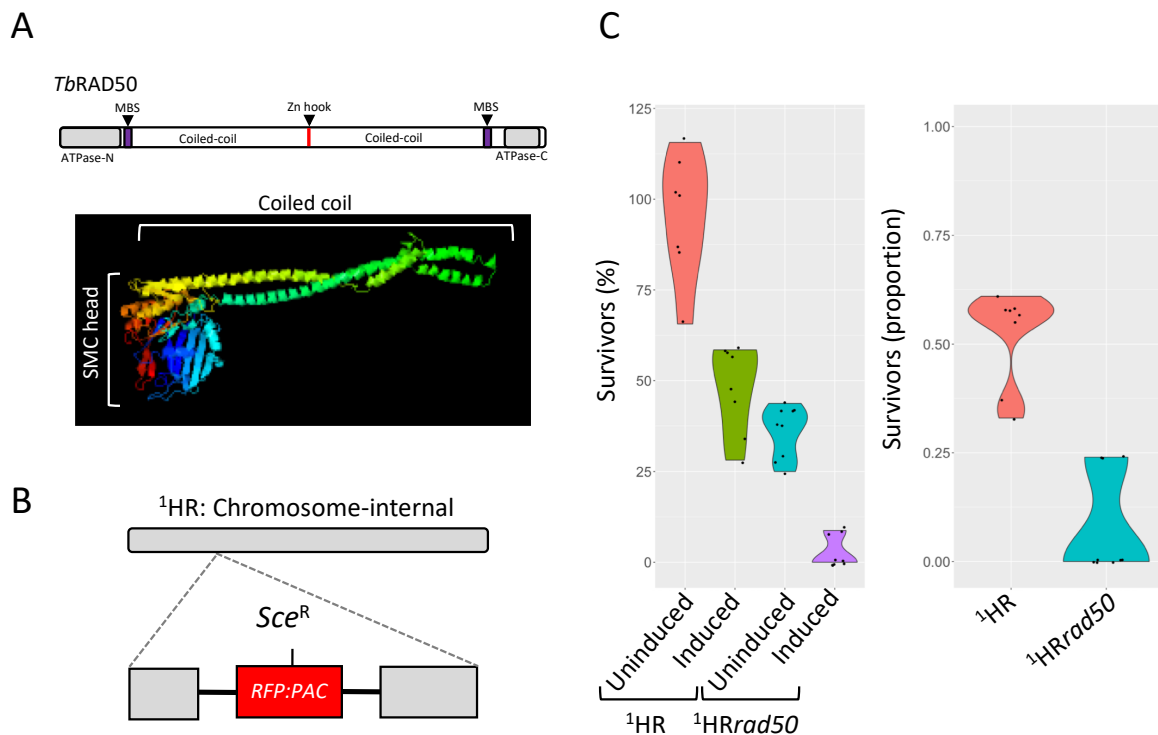
235 RAD50 is required for normal cell growth and DSB repair.

236

237 RAD50, the largest component of the MRN complex, belongs to the structural maintenance of
238 chromosomes (SMC) family of proteins⁴⁸ and has not been examined in *T. brucei*, though the gene
239 has been reported to be essential in *Leishmania infantum*⁴⁹. The domain architecture of RAD50 is
240 approximately palindromic (Figure 1A) and characterized by the presence of ATP-binding cassette
241 (ABC)-ATPase domains at the N- and C- termini, each followed by an MRE11 binding site (MBS), and
242 then by anti-parallel coiled-coil regions, which form linker structures that enable the MRN complex to
243 act as a tethering scaffold to hold broken chromosomes together for repair⁵⁰. Between the antiparallel
244 coiled-coils, a central Zn hook, a CxxC motif, facilitates Zn²⁺ dependent RAD50-RAD50 subunit
245 interactions and is presumed to be important for tethering⁵¹. A conformational change is invoked
246 through binding of RAD50 to two ATP molecules, which then allows for binding to DNA⁴³. Primary
247 sequence comparison suggested all RAD50 domains are recognisably conserved in the putative *T.*
248 *brucei* RAD50 homologue (Tb.927.11.8210; Supplementary Figure 1). Within the ATPase domains,
249 the ABC nucleotide binding domain is defined by the conserved presence of Walker A, Q-loop,
250 Signature, Walker B, D-loop, and H-loop motifs required to form the active ATPase site⁵².
251 Furthermore, structure prediction using Phyre²⁵³ modelled 503 residues (37 % of the sequence) of the
252 *T. brucei* protein, revealing a SMC head domain and antiparallel coiled coil regions (Figure 1A).

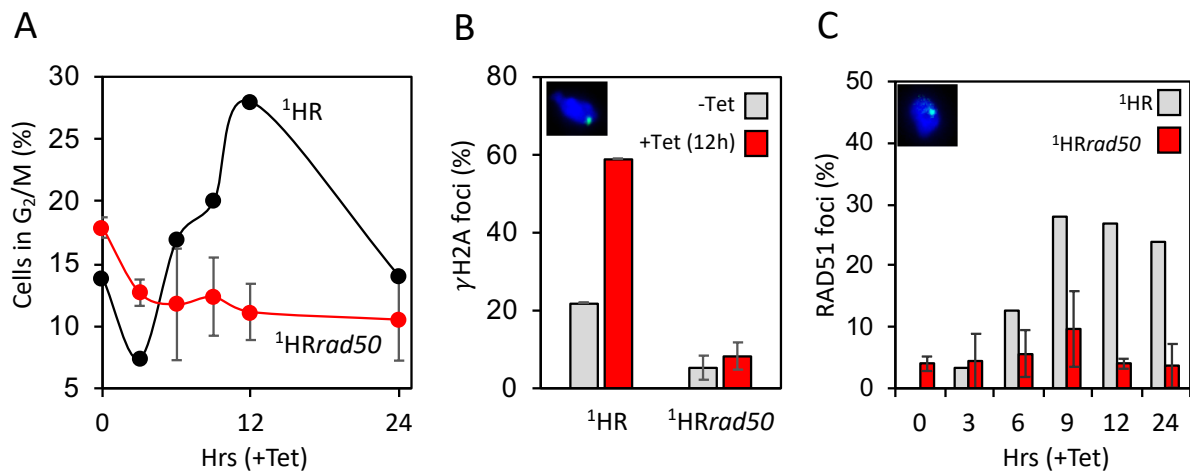
253 To test the function of RAD50 in DSB repair, we used a previously validated *T. brucei* cell line,
254 referred to as ¹HR (Figure 1B), where a single I-SceI meganuclease DSB can be induced in an *RFP-*
255 *PAC* (red fluorescent protein – puromycin *N*-acetyltransferase) fusion cassette in the core region on
256 chromosome 11¹⁷ (Figure 1B). We generated *rad50* null mutants (referred to as ¹HR*rad50*) in these
257 cells by sequentially replacing the two gene alleles with neomycin phosphotransferase (*NEO*) and
258 blasticidin (*BLA*) resistance cassettes: PCR analysis of double antibiotic resistant clones confirmed
259 *RAD50* loss and replacement (Supplementary Figure 2A and B) and demonstrates RAD50 is not
260 essential in *T. brucei*. To determine the role RAD50 plays in DNA repair, we set up clonogenic assays.
261 Cells were distributed across 96-wells plates under both I-SceI non-inducing and inducing conditions,
262 and wells with live cells scored after 5 -7 days. This revealed a significant growth defect in the
263 ¹HR*rad50* null cells in unperturbed cells (Figure 1C Left panel and Table 1): 95 % of the WT ¹HR cells
264 survived compared with ~ 35 % of the ¹HR*rad50* cells, revealing a 2.6 - fold decrease in cell survival.
265 This growth impairment is likely due to the inability to repair spontaneous DSBs. Induction of the I-SceI
266 meganuclease results in ~ 95 % cutting and repair mainly by homologous recombination¹⁷. Consistent
267 with previous findings, in the WT ¹HR strain ~ 48 % of cells are able to repair the DSB and survive
268 (Figure 1C Left panel and¹⁷ and Table 1), whereas in the ¹HR*rad50* cells, a severe growth defect was
269 seen following a DSB, with less than 3 % survival (a 16 – fold reduction), suggesting a significant
270 defect in DSB repair (Figure 1C Left panel and Table 1). This was recapitulated when assessing the
271 normalised survival efficiency (compared to uninduced survival) following an I-SceI break (Figure 1C

272 right panel and Table 1), indicating that a DSB is more lethal in the null mutant cells. In parallel we
 273 also tested the function of MRE11, as it forms a complex with RAD50, by generating null mutants
 274 through sequentially replacing the two gene alleles with *NEO* and *BLA* resistance cassettes; PCR
 275 analysis confirmed *MRE11* loss and replacement (Supplementary Figure 2C). The *mre11* nulls
 276 (referred to as ¹HR*mre11*) also showed a growth defect cells in the unperturbed cells, with only 47 %
 277 of cells surviving cloning. Induction of the I-SceI meganuclease resulted in a severe growth defect,
 278 with less than 2 % survival, suggesting a significant defect in DSB repair (Supplementary Figure 4A
 279 and Table 1) whose magnitude was very similar to ¹HR*rad50* cells, which is expected given they have
 280 been shown to act in complex in other systems^{37,38}.
 281



282
 283
 284 **Figure 1:** RAD50 is essential for DSB response and repair at a chromosome-internal locus. (A) Upper
 285 panel: Schematic of TbRAD50 with protein domains. Amino acid position of conserved domains are:
 286 ATPase - N, 4 – 170; MRE11 binding site (MBS), 182 – 205; Zn hook, 690 – 693; MRE11 binding site,
 287 1158 – 1181; ATPase - C, 1243 – 1333. Lower panel: The structure of the *T. brucei* RAD50 was
 288 modelled using Phyre2 showing the SMC head domain with a coiled coil. (B) Schematic of the
 289 chromosome-internal DSB cell line with the I-SceI recognition site, *Sce*^R, highlighted. (C) A clonogenic
 290 assay reveals survivors following a DSB at a chromosome-internal locus in the parental and ¹HR*rad50*
 291 cell lines. Cells were plated out into media with or without tetracycline. The proportion of survivors was
 292 calculated by dividing the number of induced survivors by uninduced. R:P, red fluorescent protein:
 293 puromycin fusion gene. ¹HR technical replicates; n=2, and with ¹HR*rad50* biological replicates for the
 294 strains; n=2.
 295

296 We next asked what effect of the loss of RAD50 had on the mechanisms by which
 297 trypanosomes recognize a DSB lesion and initiate a signalling cascade resulting in DNA repair⁵⁴. In
 298 *T. brucei*, the DDR after an I-SceI induced DSB has been characterized thus far to include an increase
 299 of cells in G₂/M¹⁷, phosphorylation of histone H2A⁵⁵, break resection and accumulation of RAD51 foci
 300 at the site of the DSB¹⁷. The cell cycle distribution of WT^{1HR} and ^{1HR}*rad50* cells was assessed
 301 following induction of a DSB. In WT^{1HR} cells ~28% were in G₂ 12 hours after I-SceI induction and
 302 this returned to background levels (~15% of the population) by 24 hours. In contrast, no increase in G₂
 303 cells was seen after DSB induction in the ^{1HR}*rad50* cells (Figure 2A), suggesting RAD50 is required
 304 for eliciting the G₂/M checkpoint. In mammals the MRN complex recruits the ATM kinase to a DSB,
 305 where it phosphorylates H2AX³⁷.
 306

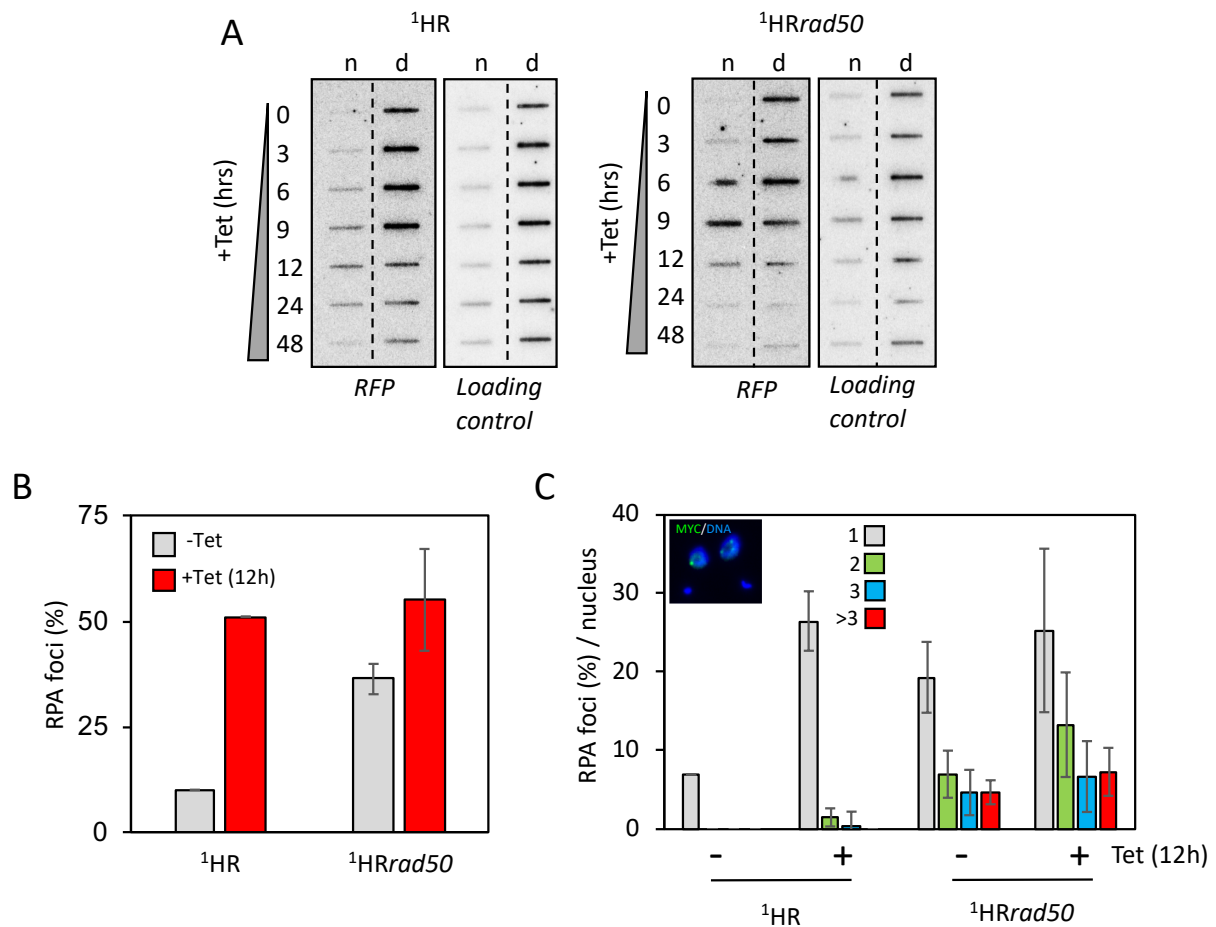


307
 308 **Figure 2:** DNA damage response is compromised in ^{1HR}*rad50* cells. (A) The number of cells in G₂/M
 309 phase cells was counted by DAPI staining at several points following induction of an I-SceI break in.
 310 G₂ cells contain one nucleus and two kinetoplasts. (B) Immunofluorescence assay to monitoring γ H2A
 311 foci. The number of positive nuclei were counted in uninduced cells and 12 hours post DSB. Inset
 312 showing a nucleus with a γ H2A focus. n = 200 for each time point in the ^{1HR} cell line and n= 400 for
 313 the ^{1HR}*rad50* strain. Error bars, SD, for ^{1HR}*rad50* biological replicates for the strains; n=2. (C)
 314 Immunofluorescence assay to monitoring RAD51 foci. The number of positive nuclei were counted in
 315 uninduced cells and 12 hours post DSB. Inset showing a nucleus, with a single RAD51 focus. n = 200
 316 for each time point in the ^{1HR} cell line and n= 400 for the ^{1HR}*rad50* strain. Error bars, SD, for
 317 ^{1HR}*rad50* biological replicates for the strains; n=2.
 318

319 Using an antibody specific to the Thr130 phosphorylated form of *T. brucei* H2A, γ H2A⁵⁵, we
 320 saw the expected background staining of ~15 – 20% of nuclei with foci in unperturbed WT ^{1HR} cells,
 321 which increased to ~60% at 12 hours post I-SceI induction (Figure 2B). In the ^{1HR}*rad50* cells, the
 322 background level of γ H2A foci was reduced to 5%, and the DSB-induced increase was drastically
 323 impaired (Figure 2B), with only 8% of cells containing γ H2A foci. Repair at this locus is predominately
 324 via RAD51-dependent homologous recombination¹⁷, and so we next assessed RAD51 foci assembly

325 following DSB induction. In the WT ¹HR strain, the number of detectable foci increased from 0 to 27%
 326 within 9 – 12 hours after I-SceI induction. In contrast, in ¹HR*rad50* cells the background level of
 327 RAD51 foci, before I-SceI induction, was higher at 4%, and only increased to 10 % (~3 fold reduced)
 328 in response to a DSB (Figure 2C). Like the ¹HR*rad50* cells, we detected fewer γ H2A foci in ¹HR*mre11*
 329 cells following a DSB (no foci detected, Supplementary Figure 4B) and a significant reduction in the
 330 number of RAD51 foci (14% compared with 36% in WT, Supplementary Figure 4B) and a loss of the
 331 G₂/M checkpoint (8.5% compared with 28% in WT, Supplementary Figure 4B). These results reveal an
 332 important role for RAD50 and MRE11 in the DDR to a DSB in trypanosomes at a single copy locus
 333 and suggest wider roles in tackling spontaneous DNA damage.

334 RAD50 restricts resection during allelic recombination.



335
 336 **Figure 3: RAD50 directs resection at chromosome-internal locus.** (A) Accumulation of ssDNA was
 337 monitored using slot-blot. Genomic DNA was extracted as indicated following I-SceI induction. Ninety
 338 percent of the sample was ‘native’ (n; ssDNA) and ten percent was denatured (d). Probe *RFP* and the
 339 loading control are described in the materials and methods. (B) Immunofluorescence assay to
 340 monitoring RPA foci. The numbers of positive nuclei were counted in uninduced cells and 12 hours
 341 post DSB. n = 200 for each time point in the ¹HR cell line and n= 400 for the ¹HR*rad50* strain. Error
 342 bars, SD, for ¹HR*rad50* biological replicates for the strains; n=2. (C) Immunofluorescence assay to
 343 monitor the number of RPA foci per nucleus. The number of RPA foci was counted in uninduced cells
 344 and 12 hours post DSB. n = 200 nuclei for each time point in the ¹HR cell line and n= 400 nuclei for

345 the ¹HR*rad50* cells. Inset showing representative nuclei, with RPA foci. Error bars, SD, for ¹HR*rad50*
346 biological replicates for the strains; n=2.

347

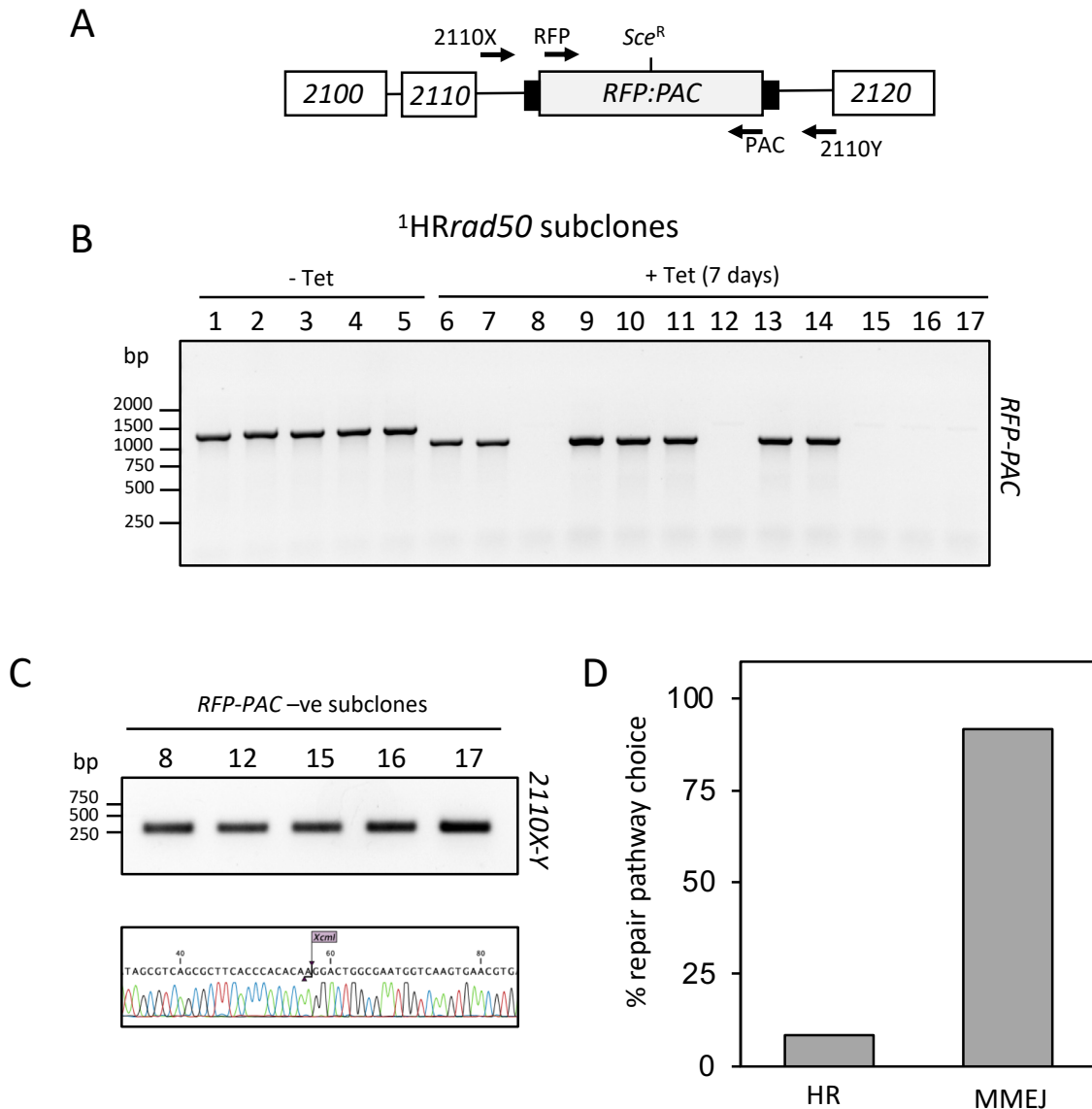
348 An early step in the DSB repair cycle is the formation of extensive 3' ssDNA overhangs,
349 initiated by MRE11 3' – 5' nuclease activity, which are a substrate for RAD51 nucleoprotein filament
350 formation and act as a template for homology-directed repair³⁷. In light of the reduced accumulation of
351 RAD51 foci after DSB induction in the absence of RAD50, we sought to determine whether the
352 formation of ssDNA at the I-SceI target locus was compromised, using slot blots. In the WT ¹HR cells,
353 ssDNA accumulated up to 12 h after I-SceI induction and declined thereafter (Figure 3A), mirroring the
354 phosphorylation of H2A and accumulation of RAD51 (Figure 2 B and C)¹⁷. Processing of the DSB in
355 the ¹HR*rad50* cells appeared to be accelerated, with ssDNA signal peaking at 9 hours and declining
356 thereafter (Figure 3A and Supplementary Figure 3). We conclude that DNA resection is not lost in the
357 ¹HR*rad50* cells but the timing is affected, though we cannot say if the extent of resection is changed.
358 Prior to RAD51 loading on to ssDNA, the trimeric RPA (replication protein A) complex binds the
359 ssDNA and is subsequently displaced by RAD51⁵⁶. Rescue of the *BLA* selectable marker in this strain
360 (Supplementary Figure 2) allowed tagging of RPA2 with the myc epitope and subsequent localization.
361 In WT ¹HR cells the number of nuclei with RPA foci increased 5-fold (from 10% to 50%) following an I-
362 SceI break (Figure 3B). The ¹HR*rad50* cells showed a pronounced increase in RPA foci prior to
363 induction of a DSB, and only a marginal increase at 12 hours post DSB (~30% - 55%; Figure 3B). In
364 the WT ¹HR cells, a single RPA focus is most commonly seen in response to an I-SceI break²².
365 However, we observed multiple RPA foci in both induced and uninduced ¹HR*rad50* null cells (Figure
366 3C). We therefore tentatively conclude that most RPA signal in the ¹HR*rad50* cells²² represents
367 persistent, widespread damage, meaning it is unclear if loss of RAD50 alters the accumulation of RPA
368 at the I-SceI induced DSB in chromosome 1.

369 RAD50 is crucial for homologous recombination in *T. brucei*

370

371 To explore how trypanosomes repair a DSB in the ¹HR*rad50* nulls, DSB-survivors from the clonogenic
372 assay were scored for repair by homologous recombination or MMEJ by a PCR assay (Figure 4A)
373 using sets of primers that flanked the *RFP-PAC* cassette. In the surviving subclones, sensitivity to
374 puromycin is indicative of cleavage by I-SceI¹⁷. All twelve of the surviving subclones were sensitive to
375 puromycin, indicating cleavage by I-SceI¹⁷ and disruption of the *RFP:PAC* cassette (data not shown).
376 Eleven of these clones showed repair by MMEJ, as seen by the reduction in the size of the PCR
377 product as compared to the controls (Figure 4B, RFP and PAC primer pair¹⁷), or loss of the entire
378 cassette (Figure 4C, 2110X and 2110Y primer pair⁵⁷). Sequencing revealed repair by MMEJ using
379 the *Xcm1* sites that flanked the *RFP-PAC* cassette in clones 12, 15, 16 and 17 (Figure 4C lower
380 panel). Sequencing of the 2110X-Y product in clone 8 revealed repair using the homologous template,
381 suggesting homologous recombination can still occur, although is significantly impaired. In the *mre11*
382 nulls, 14 out of 15 clones repaired by MMEJ (Supplementary Figure 4C, clone 10, 17 and 19 show a
383 PCR product of reduced size and for the remaining clones the 2110XY PCR product was sequenced
384 revealing 11 clones had repaired by MMEJ). These data show a significant shift in the pathway used

385 to repair a DSB in the ¹sHRad50 and ¹HRmre11 null cells at a chromosome-internal locus, with repair
 386 by MMEJ dominating (Figure 4D), compared with the pronounced predominance of homologous
 387 recombination in WT ¹HR cells ¹⁷.



388

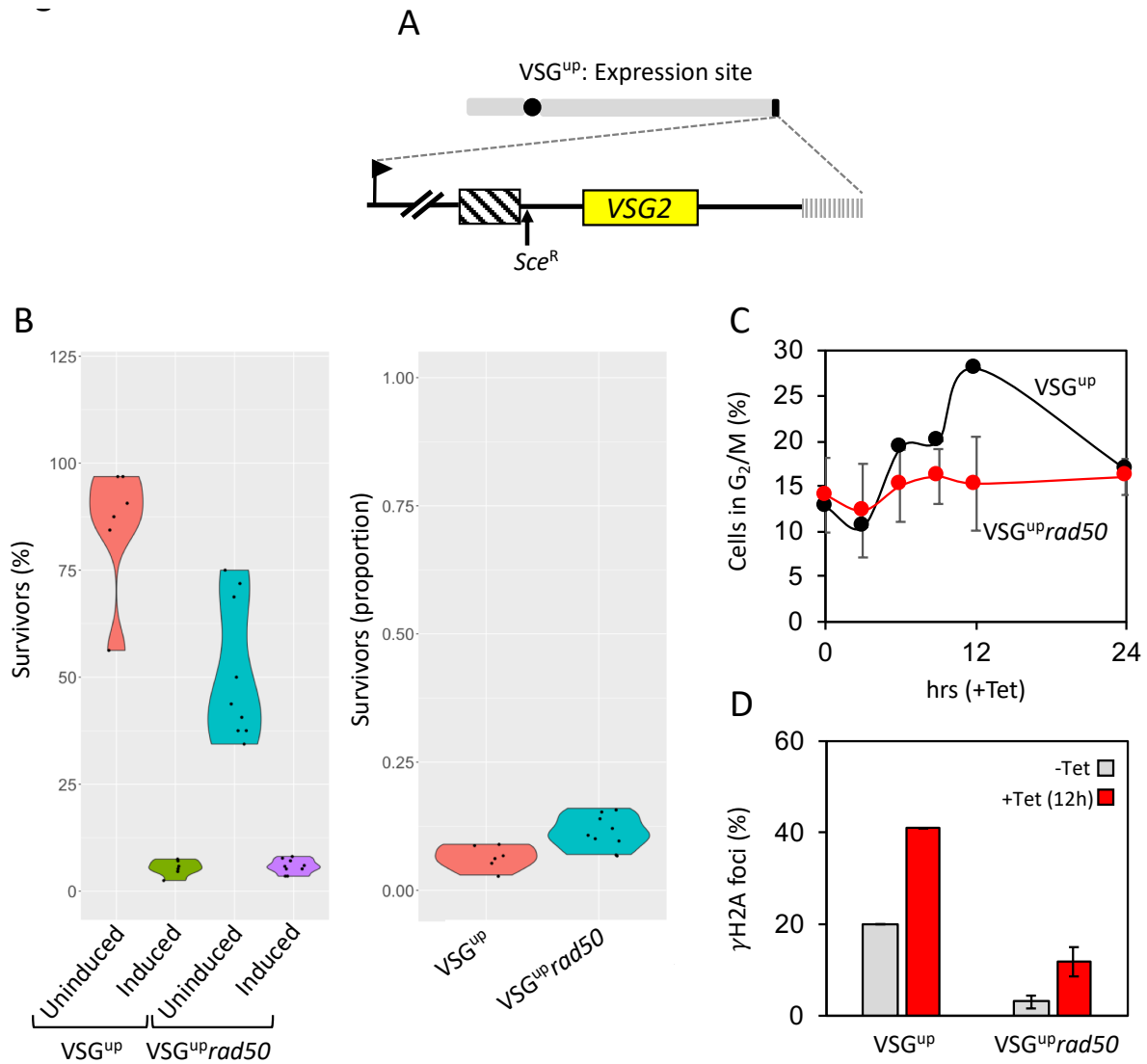
389 **Figure 4:** RAD50 is required for homologous recombination. PCR analysis of ¹HR repaired
 390 subclones. (A) Schematic showing the 2110 locus and position of the *Sce* recognition site (*Sce*^R).
 391 Position of primers indicated by arrows. Primer sequence detailed in materials and methods. (B) PCR
 392 assay of repaired subclones showing *RFP:PAC* presence or absence. (C) Upper panel: PCR assay of
 393 repaired subclones that were negative for *RFP:PAC*. Lower panel: Sanger Sequence trace showing
 394 XcmI site. (D) Percentage of survivors for each repair pathway choice. n= 12 clones. Arrows indicate
 395 position of primers. White box, genes; Grey box, *RFP – PAC* fusion gene; black box, UTRs.

396 Loss of RAD50 increases survival following a DSB at the active VSG-ES.

397

398 Trypanosomes rely on homologous recombination to facilitate antigenic variation. We therefore
399 wanted to test the role of RAD50 in VSG switching. We generated *RAD50* nulls in a cell line where the
400 I-SceI recognition site is fused to a *puromycin* selectable marker and inserted immediately
401 downstream of the major block of 70-bp repeats and upstream of VSG2 in Bloodstream form
402 Expression site 1 (BES1) (on chromosome 6a), the active VSG-ES in this strain (Figure 5A). The
403 resulting cell line is known as VSG^{up} ²⁷. Cell survival following a DSB at this position is contingent
404 upon VSG switching, most commonly using the 70-bp repeats and replacing the active VSG via break-
405 induced replication ^{26,27}. We generated *rad50* null VSG^{up} strains (VSG^{up}*rad50*), by replacing the two
406 gene alleles with *NEO* and *BLA* resistance cassettes: PCR analysis of double antibiotic resistant
407 clones confirmed *RAD50* loss and replacement (Supplementary Figure 2A and B). Using a clonogenic
408 assay we found that, like in the ¹HR strain, there was a growth defect (1.6-fold reduction) in the
409 VSG^{up}*rad50* nulls compared with VSG^{up} WT cells in the absence of I-SceI induced damage (Figure
410 5B; left panel and Table 1). This effect again suggests an impaired ability to repair spontaneous
411 damage within the mutant cell. However, quite differently to ¹HR cells, following induction of an I-SceI
412 DSB we observed an increase in survival in the VSG^{up}*rad50* nulls compared with induced VSG^{up} WT
413 cells (Figure 5B; left panel and Table 1). These data indicate that RAD50 suppresses DSB repair at a
414 VSG-ES, the opposite of its role at a chromosome-internal DSB. In contrast, survival is reduced in the
415 VSG^{up} *mre11* nulls relative to VSG^{up} WT, with only 1.75% able to survive a DSB (Supplementary
416 Figure 6A and Table 1). We then assessed the DDR in the VSG^{up} cell line. As in the ¹HR cells,
417 following a DSB, the number of cells that accumulate in G₂/M increases to ~ 30 % in the VSG^{up} WT
418 cell line ²⁷, and this cell cycle checkpoint was lost in the VSG^{up}*rad50* cells (Figure 5C) and in the
419 VSG^{up}*mre11* cells (Supplementary Figure 6B). In the VSG^{up} WT cell line, the number of γ H2A foci
420 increased from 20% to 41% after I-SceI induction, as has been previously reported ²⁷. In the
421 VSG^{up}*rad50* nulls, γ H2A foci were only detected in 3% of uninduced cells, and this increased to 11%
422 following a DSB (Figure 5D). A similar phenotype was seen in the VSG^{up}*mre11* cells, with the number
423 of γ H2A foci increasing from 1.3% to 7% (Supplementary Figure 6B). Thus, while it appears that loss
424 of RAD50 or MRE11 diminishes the capacity of cells to phosphorylate H2A in response to a DSB at
425 this locus, the increased survival in the VSG^{up}*rad50* cells suggests that while it is required for an
426 efficient DDR, in its absence the cells are more adept at repair.

427 Using a series of assays (Figure 6A and Supplementary figure 5) we next looked at DNA
428 rearrangements in the VSG-ES to determine how the VSG^{up}*rad50* cells repair an induced DSB. 25
429 subclones were selected from the clonogenic assay and tested for sensitivity to puromycin, asking
430 about the frequency of loss of the puromycin gene from the VSG-ES. 24 out of 25 subclones were
431 sensitive to 1 μ g.ml⁻¹ puromycin, indicating that the majority of the population had been subject to a
432 DSB and had deleted the resistance cassette. Immunofluorescence using antibodies against VSG2,
433 the VSG expressed from the modified VSG-ES, showed that 23 out of 24 puromycin sensitive
434 subclones had switched VSG (Figure 6B). This is comparable to what is seen in the VSG^{up} WT strain,
435 suggesting loss of RAD50 does not affect the cell's ability to undergo VSG switching. The single
436 puromycin resistant clone was VSG2 positive, suggesting I-SceI did not cut (Supplementary Figure 5,
437 subclone 14).



438

439

440 **Figure 5:** RAD50 suppresses repair at a subtelomeric locus. (A) A schematic of the active expression

441 site DSB cell line with the I-SceI recognition site, Sce^R, highlighted. (B) A clonogenic assay reveals the

442 survivors following a DSB at the active expression site in the parental and VSG^{UP}rad50 cell lines. Cells

443 were plated out into media with or without tetracycline and counted after seven days. Other details as in

444 Figure 1. (C) The number of cells in G₂/M phase cells was counted by DAPI staining at 0 hours and

445 12 hours following induction of an I-SceI break in. G₂ cells contain one nucleus and two kinetoplasts.

446 (D) Immunofluorescence assay to monitoring γH2A foci. The nuclei with γH2A foci were counted in

447 uninduced cells and 12 hours post DSB. n = 200 for each time point in the VSG^{UP} cell line and n= 400

448 for the *RAD50* null. Error bars, SD, for VSG^{UP}rad50 biological replicates for the strains; n=2. Arrow,

449 RNA Pol 1 promoter; box with diagonal lines, 70-bp repeats; vertical lines, telomere.

450

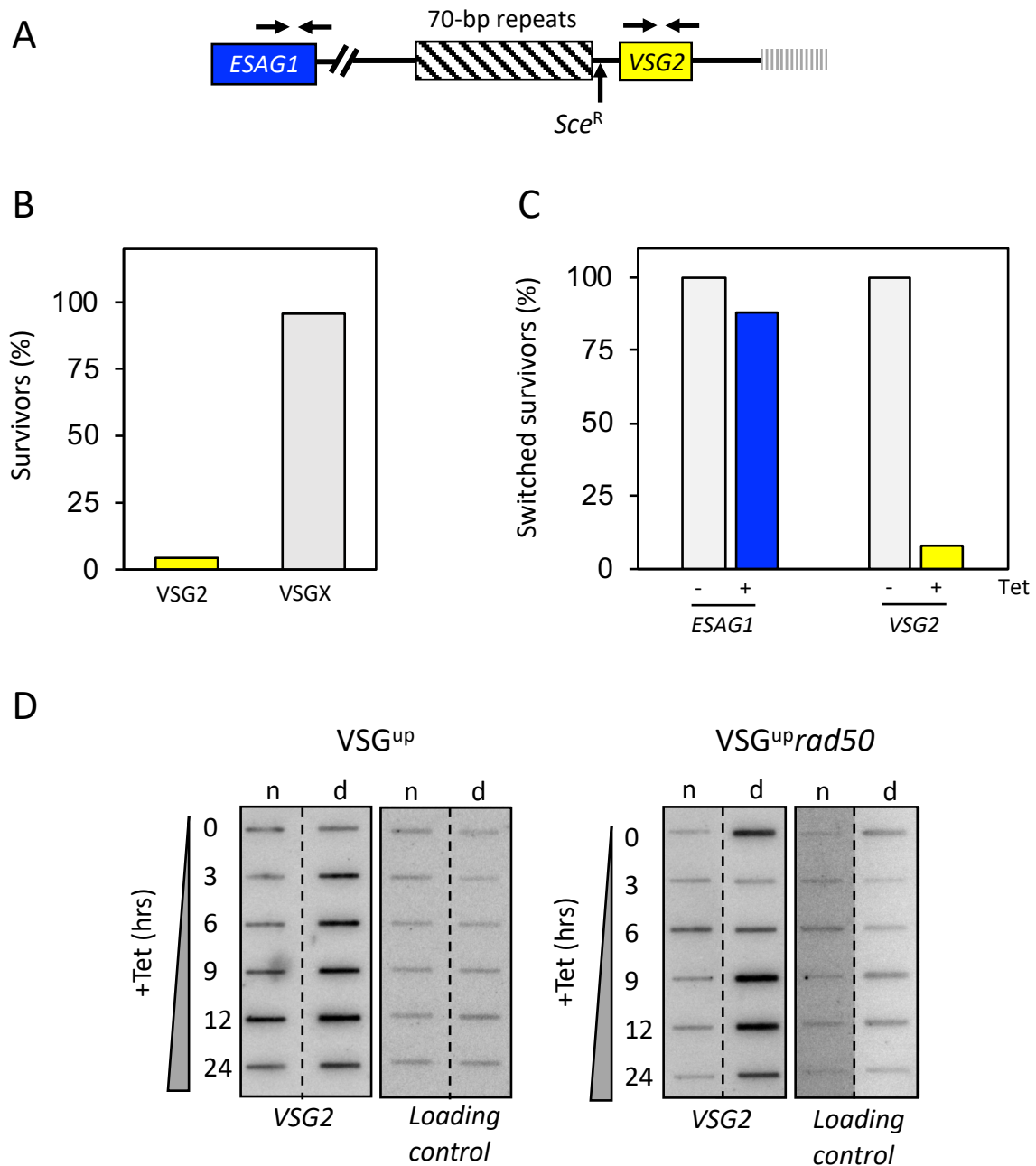
451 We then looked at DNA rearrangements in the ES using primers specific to *VSG2* and *ESAG1*.

452 *ESAG1* is found upstream of a block of 70-bp repeats in the active VSG-ES and cells that retain

453 *ESAG1* are presumed to have repaired by gene conversion using the 70-bp repeats. Both *VSG2* and

454 *ESAG1* were retained in five out of five uninduced control subclones (Figure 6C and Supplementary

455 Figure 3). Of the 24 puromycin sensitive subclones (i.e. cleaved by I-SceI), *ESAG1* was retained in 23
 456 and *VSG2* was lost in 23 (Figure 6C and Supplementary Figure 5).



457
 458 **Figure 6:** RAD50 is not required for VSG switching . (A) A schematic map shows the primer position
 459 at the active expression site. (B) Immunofluorescence assay for VSG2, showing the percentage of
 460 switched survivors in the VSG^{up}*rad50* cell line. (C) PCR analysis shows the percentage of switched
 461 survivors that kept *ESAG1* and *VSG2*. n= 24 clones. Arrows indicate position of primers; box with
 462 diagonal lines, 70-bp repeats; vertical lines, telomere. (D) Accumulation of ssDNA was monitored
 463 using slot-blots. Genomic DNA was extracted as indicated following I-SceI induction. Ninety percent
 464 the sample was 'native' (n; ssDNA) and ten percent was denatured (d). Probe *VSG2* and the loading
 465 control are described in the materials and methods.

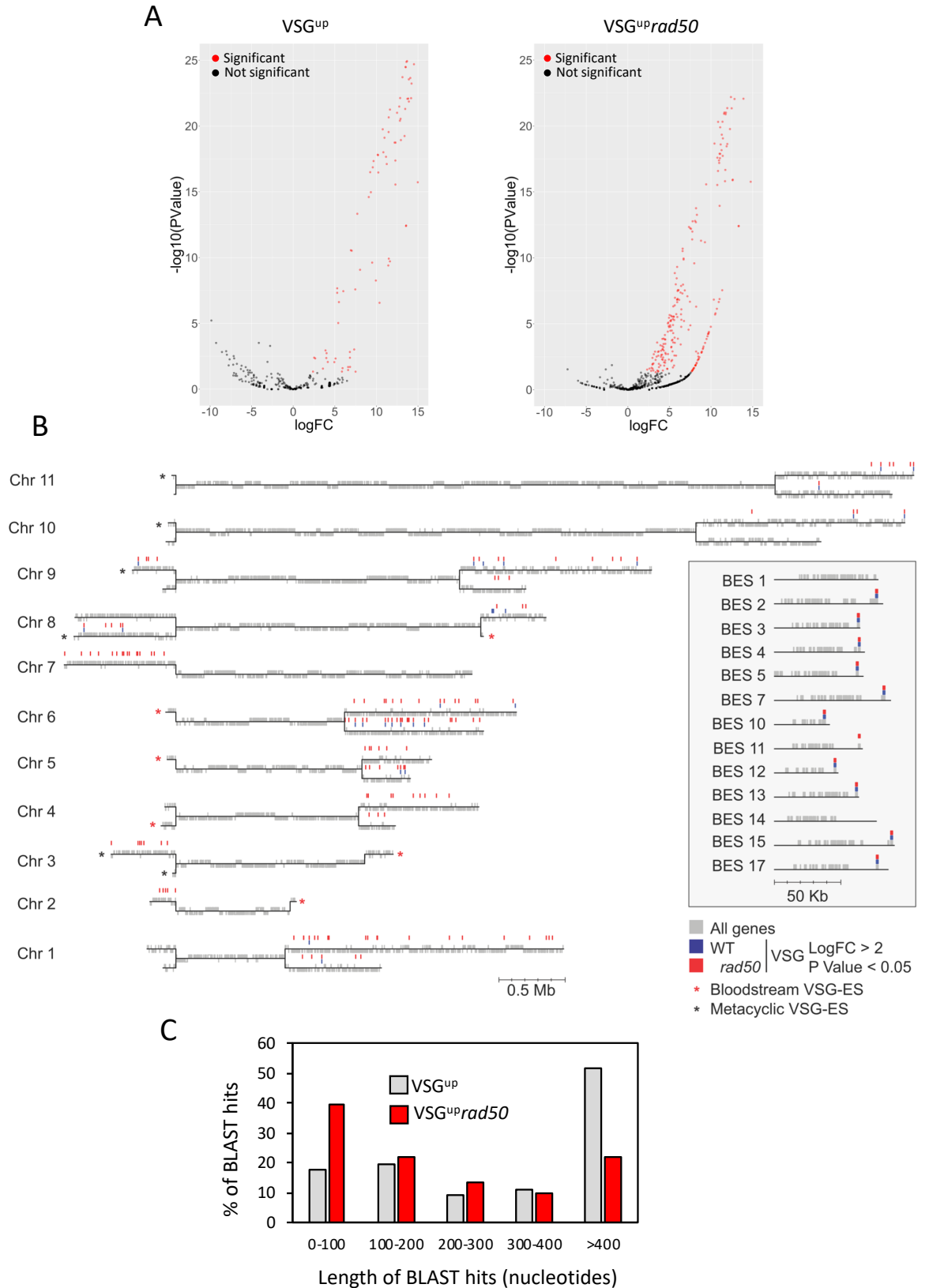
466 One subclone was found to be VSG2 negative by immunofluorescence, puromycin sensitive,
467 and *ESAG1* positive and VSG2 positive by PCR. This suggests that this single clone had switched by
468 *in situ* transcriptional activation of another VSG-ES (Figure 6B and C and Supplementary Figure 3),
469 whereas all other clones had undergone VSG switching by recombination. In the VSG^{up}*mre11* cells, all
470 the puromycin sensitive subclones had switched VSG and lost the VSG2 gene as seen by PCR
471 analysis (Supplementary Figure 4C). 18 out of the 20 subclones had also retained *ESAG1*. As with
472 the VSG^{up}*rad50* cells, these clones are presumed to have repaired by gene conversion using the 70-
473 bp repeats. We then assessed the formation of ssDNA and found that as in the ¹HR*rad50* nulls, the
474 formation of ssDNA was not abolished but seemed to accumulate earlier - here at 6 hours post DSB
475 induction (Figure 6D). These data suggest that loss of RAD50 or MRE11 does not impair the cell's
476 ability to undergo switching by DNA recombination.

477

478 RAD50 promotes recombination using long stretches of homology.

479

480 Increased survival of the VSG^{up}*rad50* nulls after induction of a DSB suggested a hyper-
481 recombinogenic mechanism in this locus, through which the cells are able to repair and switch at a
482 higher rate than in the parental cell line. One explanation for such enhanced repair could be through
483 greater access to the silent VSG repertoire. In the *T. brucei* genome there are in excess of 2000 VSG
484 genes found at the subtelomeric arrays^{1613,15,58}, 90% of which are associated with a stretch of 70-bp
485 repeat sequence¹⁴ that can be used for homology during repair⁹. To ask if differences in VSG
486 repertoire access explains increased survival of VSG^{up}*rad50* cells after DSB induction, we used VSG-
487 seq¹⁰. In the VSG^{up} WT cell line, 83 VSG gene transcripts were significantly enriched in the induced
488 cells compared with uninduced (Figure 7A) (greater than 2 log₂ fold change and *p* value of less than
489 0.05). In the VSG^{up}*rad50* cell line, a greater number of VSGs were detected: here 225 VSG transcripts
490 were significantly enriched after I-SceI induction (Figure 7A). To understand this increase, we then
491 looked at the genomic position of the VSG cohorts. In the VSG^{up} cells, we found that approximately
492 equal numbers of enriched VSGs mapped to the VSG-ES and minichromosomes relative the
493 megabase arrays, despite the much greater number of genes in the latter component of the archive
494 (Figure 7B, Supplementary Figure 7A). These data appear consistent with VSG switching having
495 followed a loose hierarchy, as previously published⁵⁹, with telomeric VSG preferred as donors. In the
496 VSG^{up}*rad50* cell line, enriched VSG genes also mapped to the VSG-ESs, minichromosomes and
497 megabase arrays, but a significantly higher proportion (67% compared with 34% in WT) were from
498 subtelomeric arrays (Figure 7B, Supplementary Figure 7A). This suggests that the VSG^{up}*rad50* cells
499 are able to access a greater proportion of the silent VSG archive for repair and VSG switching.
500 To ask if increased VSG switching in the absence of RAD50 could be explained by changes in the
501 mechanism of recombination, we looked at the length of homology used for repair. Using BLAST
502 analysis, we queried the significantly enriched VSGs against the telomeric end of BES1, searching for
503 regions of homology (Figure 7C and Supplementary Figure 7B). This analysis revealed that, compared
504 with the VSG^{up} WT cells, VSG genes activated in the VSG^{up}*rad50* cells shared shorter stretches of
505 homology with the active VSG2 locus.



506
507

508 **Figure 7: RAD50 restricts antigenic variation.** (A) Volcano plots of VSG-seq showing log₂ fold change
509 vs. log₁₀ P value for VSG^{up} and VSG^{up}rad50 strains. Red genes are significantly up-regulated (P value
510 < 0.05 and log₂ FC > 2). (B) *T. brucei* 427 Genome map showing all 11 megabase chromosomes in

511 black lines and all genes in grey. Significantly up-regulated VSG genes from either VSG^{up} (blue) or
512 VSG^{up}rad50 (red). Inset box shows all 13 BES with significantly up-regulated VSG genes from either
513 VSG^{up} (blue) or VSG^{up}rad50 (red). (C) Chromosome 6 map showing all genes in grey and significantly
514 up-regulated VSG genes from either VSG^{up} (blue) or VSG^{up}rad50 (red). (C) Percentage usage for the
515 length of the BLAST hits from either VSG^{up} (blue) or VSG^{up}RAD50 (red). Box with diagonal lines, 70-bp
516 repeats; vertical lines, telomere; grey box, 3'UTR

517

518 The most commonly used length of homology in the VSG^{up}rad50 cells was 100 bp (40% of survivors),
519 whereas the VSG^{up}WT cells most frequently used >400 bp (51% of survivors) (Figure 7C). Thus,
520 increased survival in the absence of RAD50 is due to increased access to archival VSGs due to more
521 frequent DSB repair using short stretches of homology.

522

523 DISCUSSION

524

525 Central to the DDR and subsequent repair is the MRN complex, within which the MRE11 – RAD50
526 heterodimer forms the catalytic core. In fact, this core complex is so fundamental to repair that it is
527 conserved across bacteriophages, bacteria, archaea and eukaryotes⁶⁰. Kinetoplastids rely on
528 homology-based recombination as the major form of repair, since no data has suggested the use of
529 non-homologous end-joining after I-SceI induction of a DSB at both at chromosome-internal¹⁷ and
530 telomeric loci in *T. brucei*, or after CRISPR-Cas9 DSB formation in *Leishmania*, *T. cruzi* or *T. brucei*⁶¹⁻
531⁶³. At least in *T. brucei*, HR predominates over MMEJ after induction of a DSB¹⁷, and all evidence
532 suggests RAD51-dependent HR dominates as the major form of repair reaction during VSG switching
533 at the VSG-ES¹⁹. What dictates the preference of HR over MMEJ in these reactions in *T. brucei* and
534 related kinetoplastids is unknown. Here, we have shown that *T. brucei* RAD50 is critical for normal cell
535 growth and efficient homology-based DNA repair after induction of a DSB, which is consistent with a
536 conserved role in DSB recognition and repair. We demonstrate that in the absence of RAD50 the DDR
537 is severely compromised, as evidenced by the loss of γ H2A accumulation and the G₂/M cell-cycle
538 checkpoint at both subtelomeric and chromosome-internal DSBs, and the RPA focal accumulation.
539 We also show that HR is dependent on RAD50, as null mutants displayed compromised RAD51 foci
540 formation and switched repair pathway choice from HR to MMEJ at a chromosome-internal DSB. In
541 contrast, at a VSG-ES we demonstrate that RAD50 restrains the DDR, since in its absence break
542 processing dynamics were altered, cell survival improved and a greater diversity of VSGs were
543 activated following a DSB. Thus, this work provides insight into DSB repair pathway choice,
544 compartmentalization of repair with specific relevance for understanding trypanosome antigenic
545 variation and genome maintenance in all kinetoplastids.

546 In *T. brucei* RAD51-dependent HR accounts for approximately 95% of DSB repair at a
547 chromosome-internal locus, and a DSB triggers a conventional DDR¹⁷. The data shown here indicate
548 that the role of *T. brucei* RAD50 in recognizing a DSB and initiating the DDR appears consistent with
549 its role in other eukaryotes^{64,65}. Previous characterization of MRE11 has revealed a role in HR and
550 genomic stability in both *T. brucei*^{46,47} and *Leishmania*^{49,66}, suggesting RAD50 and MRE11 act

551 together. Here we show that that MRE11 is essential for the DDR and HR and, in its absence, repair is
552 predominantly achieved by MMEJ. We expect that the reduced survival of ¹HR*rad50* and VSG^{up}*rad50*
553 cells is due to unrepaired DNA damage that results in cell death, which is also seen in *mre11* mutants
554 ^{46,47}. The persistence of RPA foci in the ¹HR*rad50* cells is further evidence of defective repair in these
555 cells, explained by RPA remaining associated with ssDNA at sites of damage. This observation may
556 also reflect a damage tolerance strategy employed by *T. brucei* ²², but in these circumstances γ H2A
557 and RAD51 are not recruited to the break after replication, unlike what is seen in *T. cruzi* where
558 ionizing radiation tolerance is dependent on RAD51⁶⁷. DNA resection following a DSB is one of the
559 early steps in the DDR. MRN is an early acting complex in DSB processing, initiating resection^{39,68}
560 and recruiting the SGS2 nuclease and DNA2 and EXO1 for long-range resection thereafter^{39,69}. The
561 lack of resection defect in the ¹HR*rad50* mutants, coupled with the altered dynamics of the formation
562 and resolution of ssDNA, suggests that in trypanosomes there is flexibility in the nucleases able to
563 initiate and resect across a DSB and, in the absence of MRN, unknown nucleases can act in an
564 unrestricted manner that exceeds the resection rate of WT cells.

565 Loss of RAD50 in *T. brucei* reveals a striking difference in the response to a DSB at a
566 chromosome-internal location and in the active VSG-ES, with dramatically impaired survival at the
567 former and improved survival at the latter. This locus-specific effect of *rad50* nulls was not reproduced
568 in the *mre11* nulls. It is possible that this difference arises from a shared change in DSB repair
569 reaction mechanism due to loss of the MRN complex. After DSB induction, loss of RAD50 results in
570 lower levels of γ H2A and RAD51 foci, allied to more rapid formation and resolution of ssDNA at a
571 chromosome-internal site, with the result that DSB repair no longer favours HR but instead mainly
572 uses MMEJ. An explanation for these effects could be that loss of RAD50 leads to impaired DSB
573 processing by MRE11, allowing altered resection that leads to lowered levels of RAD51 nucleoprotein
574 filament formation and increased recruitment of the unknown *T. brucei* machinery for MMEJ. If the
575 MMEJ reaction was more efficient than HR, the more rapid resolution of ssDNA would be explained. If
576 this same redirection of DSB repair occurred in the VSG-ES, why might the difference in survival
577 occur? A simple explanation might be that MMEJ repair is more error-prone (such as by mutation or
578 translocation) than HR⁷⁰, and the use of error-prone MMEJ has a greater impact in the chromosome
579 core, where it would affect housekeeping genes, than in the subtelomeres, where there is a huge
580 abundance of silent VSG substrates. Because the machinery that directs MMEJ in *T. brucei* or any
581 kinetoplastid has not been characterised, directs tests of this suggestion are not yet possible. In
582 addition, it remains to be shown that MMEJ directs the activation of silent array VSGs after a DSB in
583 the VSG-ES, since the length of homologies we describe here (predominantly ~100 bp) appear longer
584 than the ~5-15 bp microhomologies so far detailed in experimental characterization of *T. brucei*
585 MMEJ^{21,71}. Nonetheless, previous work has shown considerable flexibility in the substrate
586 requirements of recombination in *T. brucei*⁷¹, and linked MMEJ and HR-mediated repair of a DSB has
587 been detailed²¹. Thus, it remains possible that MRN is pivotal in determining the routing of DNA repair
588 throughout the *T. brucei* genome.

589 DNA DSBs are a potent trigger for *T. brucei* antigenic variation and it has been shown that the
590 subtelomeric VSG-ES are fragile and prone to DSBs ²⁷. A DSB upstream of the active VSG triggers

591 antigenic variation, and subsequent repair by recombination is facilitated by stretches of 70-bp repeat
592 that provide homology^{9,26,27}, via either a RAD51-dependent or independent pathway²⁷. Given this, it
593 remains perplexing that mutation of MRE11 was not previously shown to alter the rate of VSG
594 switching⁴⁶, unlike the clear alteration in survival and repair pathway seen here after loss of RAD50
595 and induction of a VSG-ES DSB. These data may suggest an unconventional signalling pathway
596 following a DSB at the active VSG-ES that allows the cells to bypass the conventional MRN / ATM
597 pathway. One way that might occur is that the DSBs in the VSG-ES do not arise directly, but are
598 generated by routes such as clashes between replication and transcription³¹, or the formation of RNA-
599 DNA hybrids⁷²⁻⁷⁴, which might not elicit recruitment of MRN or ATM^{75,76}. Our data reveals that
600 increased survival in the VSG^{up}*rad50* cells is due to their ability to access more of the genomic VSG
601 archive for repair, and the repair reaction occurs as a result of recombination using shorter stretches
602 of homology. RAD50, therefore, appears to suppress antigenic variation by committing *T. brucei* to
603 RAD51-dependent repair pathway that is reliant on long stretches of donor homology. We also note
604 that we observe a striking number of donor VSG genes used for repair on Chromosome 6 – BES1,
605 which contains the I-SceI site is found on Chromosome 6a. Indeed, several other factors have also
606 been shown to suppress antigenic variation: HAT3³⁵, TOPO3 α ³² and the telomere-interacting factor
607 TIF2⁷⁷. Antigenic variation following a DSB is driven by break-induced repair^{26,27} and, in yeast, RAD51-
608 independent BIR has been shown require as little as 30 bp of homology for repair⁷⁸. Thus, loss of
609 RAD50 may allow *T. brucei* to enlist RAD51-independent BIR to respond to a DSB in the VSG-ES,
610 using shorter stretches of homology, rather than MMEJ. Irrespective, the question arises as to why *T.*
611 *brucei* might limit the range of VSGs that can be used in antigenic variation, since this appears counter
612 to the observed diversity of VSGs seen during infections^{10,11}. It is possible that RAD50-mediated
613 restraint of VSG recombination is needed to preserve the VSG archive, saving genes for use in
614 prolonged infections. A more radical possibility is that RAD50/MRN control underlies the hierarchy of
615 VSG expression, directing DSB repair to telomeric VSG substrates early an infection and then giving
616 way to a distinctly signalled reaction, such as MMEJ, that allows access to the whole VSG archive
617 later.

618

619 **DATA AVAILABILITY**

620

621 All script is hosted on GitHub : <https://github.com/LGloverTMB/DNA-repair-mutant-VSG-seq>

622 All data has been deposited onto the ENA under study accession number: PRJEB37290

623 and unique study name: ena-STUDY-INSTITUT PASTEUR-15-03-2020-20:11:26:661-115

624

625 **ACKNOWLEDGEMENTS**

626

627 A-K.M, M.P, A.D-H and L.G performed the experiments, S.H performed the VSG-Seq data analysis,

628 R.M and L.G discussed the results and wrote the manuscript. A-K.M, S.H, R. M and L.G edited the

629 manuscript. We would also like to that David Horn for discussions and support.

630

631 **FUNDING**

632 AK. M. was supported by the Erasmus + program of the European Union. Work in the L.G. laboratory
633 has received financial support from the Institut Pasteur and the National Research Agency (ANR –
634 VSGREG). Aspects of the work in this grant was support by the Wellcome Trust (089172, 206815).
635 Further work in RM's lab was supported by the BBSRC (BB/K006495/1, BB/N016165/1), and the
636 Wellcome Centre for Integrative Parasitology is supported by core funds from the Wellcome Trust
637 (104111). S.H. is a Marie Curie fellow, this project has received funding from the European Union's
638 Horizon 2020 research and innovation programme under the Marie Skłodowska-Curie grant
639 agreement No 794979

640

641

- 642 1 Trindade, S. *et al.* Trypanosoma brucei Parasites Occupy and Functionally Adapt to the
643 Adipose Tissue in Mice. *Cell Host Microbe* **19**, 837-848, doi:10.1016/j.chom.2016.05.002
644 (2016).
- 645 2 Capewell, P. *et al.* The skin is a significant but overlooked anatomical reservoir for vector-
646 borne African trypanosomes. *Elife* **5**, doi:10.7554/eLife.17716 (2016).
- 647 3 Jamonneau, V. *et al.* Untreated human infections by Trypanosoma brucei gambiense are not
648 100% fatal. *PLoS Negl Trop Dis* **6**, e1691, doi:10.1371/journal.pntd.0001691 (2012).
- 649 4 Baltz, T. *et al.* Chemical and immunological characterization of specific glycoproteins from
650 Trypanosoma equiperdum variants. *FEBS Lett* **82**, 93-96, doi:10.1016/0014-5793(77)80893-4
651 (1977).
- 652 5 Diffley, P. Trypanosoma brucei: immunogenicity of the variant surface coat glycoprotein of
653 virulent and avirulent subspecies. *Exp Parasitol* **59**, 98-107, doi:10.1016/0014-
654 4894(85)90062-1 (1985).
- 655 6 Schwede, A., Jones, N., Engstler, M. & Carrington, M. The VSG C-terminal domain is
656 inaccessible to antibodies on live trypanosomes. *Mol Biochem Parasitol* **175**, 201-204,
657 doi:10.1016/j.molbiopara.2010.11.004 (2011).
- 658 7 Sima, N., McLaughlin, E. J., Hutchinson, S. & Glover, L. Escaping the immune system by
659 DNA repair and recombination in African trypanosomes. *Open Biol* **9**, 190182,
660 doi:10.1098/rsob.190182 (2019).
- 661 8 Hertz-Fowler, C. *et al.* Telomeric expression sites are highly conserved in Trypanosoma
662 brucei. *PLoS One* **3**, e3527, doi:10.1371/journal.pone.0003527 (2008).
- 663 9 Hovel-Miner, G., Mugnier, M. R., Goldwater, B., Cross, G. A. & Papavasiliou, F. N. A
664 Conserved DNA Repeat Promotes Selection of a Diverse Repertoire of Trypanosoma brucei
665 Surface Antigens from the Genomic Archive. *PLoS Genet* **12**, e1005994,
666 doi:10.1371/journal.pgen.1005994 (2016).
- 667 10 Mugnier, M. R., Cross, G. A. & Papavasiliou, F. N. The in vivo dynamics of antigenic variation
668 in Trypanosoma brucei. *Science* **347**, 1470-1473, doi:10.1126/science.aaa4502 (2015).
- 669 11 Hall, J. P., Wang, H. & Barry, J. D. Mosaic VSGs and the scale of Trypanosoma brucei
670 antigenic variation. *PLoS Pathog* **9**, e1003502, doi:10.1371/journal.ppat.1003502 (2013).

- 671 12 Jayaraman, S. *et al.* Application of long read sequencing to determine expressed antigen
672 diversity in *Trypanosoma brucei* infections. *PLoS Negl Trop Dis* **13**, e0007262,
673 doi:10.1371/journal.pntd.0007262 (2019).
- 674 13 Cross, G. A., Kim, H. S. & Wickstead, B. Capturing the variant surface glycoprotein repertoire
675 (the VSGnome) of *Trypanosoma brucei* Lister 427. *Mol Biochem Parasitol* **195**, 59-73,
676 doi:10.1016/j.molbiopara.2014.06.004 (2014).
- 677 14 Marcello, L. & Barry, J. D. Analysis of the VSG gene silent archive in *Trypanosoma brucei*
678 reveals that mosaic gene expression is prominent in antigenic variation and is favored by
679 archive substructure. *Genome Res* **17**, 1344-1352, doi:10.1101/gr.6421207 (2007).
- 680 15 Muller, L. S. M. *et al.* Genome organization and DNA accessibility control antigenic variation in
681 trypanosomes. *Nature* **563**, 121-125, doi:10.1038/s41586-018-0619-8 (2018).
- 682 16 Berriman, M. *et al.* The genome of the African trypanosome *Trypanosoma brucei*. *Science*
683 **309**, 416-422, doi:10.1126/science.1112642 (2005).
- 684 17 Glover, L., McCulloch, R. & Horn, D. Sequence homology and microhomology dominate
685 chromosomal double-strand break repair in African trypanosomes. *Nucleic Acids Res* **36**,
686 2608-2618, doi:10.1093/nar/gkn104 (2008).
- 687 18 McCulloch, R. & Barry, J. D. A role for RAD51 and homologous recombination in
688 *Trypanosoma brucei* antigenic variation. *Genes Dev* **13**, 2875-2888 (1999).
- 689 19 Robinson, N. P., Burman, N., Melville, S. E. & Barry, J. D. Predominance of duplicative VSG
690 gene conversion in antigenic variation in African trypanosomes. *Mol Cell Biol* **19**, 5839-5846
691 (1999).
- 692 20 Conway, C., Proudfoot, C., Burton, P., Barry, J. D. & McCulloch, R. Two pathways of
693 homologous recombination in *Trypanosoma brucei*. *Mol Microbiol* **45**, 1687-1700,
694 doi:10.1046/j.1365-2958.2002.03122.x (2002).
- 695 21 Glover, L., Jun, J. & Horn, D. Microhomology-mediated deletion and gene conversion in
696 African trypanosomes. *Nucleic Acids Res* **39**, 1372-1380, doi:10.1093/nar/gkq981 (2011).
- 697 22 Glover, L., Marques, C. A., Suska, O. & Horn, D. Persistent DNA Damage Foci and DNA
698 Replication with a Broken Chromosome in the African Trypanosome. *MBio* **10**,
699 doi:10.1128/mBio.01252-19 (2019).
- 700 23 Burton, P., McBride, D. J., Wilkes, J. M., Barry, J. D. & McCulloch, R. Ku heterodimer-
701 independent end joining in *Trypanosoma brucei* cell extracts relies upon sequence
702 microhomology. *Eukaryot Cell* **6**, 1773-1781, doi:10.1128/EC.00212-07 (2007).
- 703 24 Nenarokova, A. *et al.* Causes and Effects of Loss of Classical Nonhomologous End Joining
704 Pathway in Parasitic Eukaryotes. *MBio* **10**, doi:10.1128/mBio.01541-19 (2019).
- 705 25 Shibata, A. Regulation of repair pathway choice at two-ended DNA double-strand breaks.
706 *Mutat Res* **803-805**, 51-55, doi:10.1016/j.mrfmmm.2017.07.011 (2017).
- 707 26 Boothroyd, C. E. *et al.* A yeast-endonuclease-generated DNA break induces antigenic
708 switching in *Trypanosoma brucei*. *Nature* **459**, 278-281, doi:10.1038/nature07982 (2009).

709 27 Glover, L., Alford, S. & Horn, D. DNA break site at fragile subtelomeres determines
710 probability and mechanism of antigenic variation in African trypanosomes. *PLoS Pathog* **9**,
711 e1003260, doi:10.1371/journal.ppat.1003260 (2013).

712 28 Proudfoot, C. & McCulloch, R. Distinct roles for two RAD51-related genes in *Trypanosoma*
713 *brucei* antigenic variation. *Nucleic Acids Res* **33**, 6906-6919, doi:10.1093/nar/gki996 (2005).

714 29 Trenaman, A. *et al.* *Trypanosoma brucei* BRCA2 acts in a life cycle-specific genome stability
715 process and dictates BRC repeat number-dependent RAD51 subnuclear dynamics. *Nucleic*
716 *Acids Res* **41**, 943-960, doi:10.1093/nar/gks1192 (2013).

717 30 Hartley, C. L. & McCulloch, R. *Trypanosoma brucei* BRCA2 acts in antigenic variation and has
718 undergone a recent expansion in BRC repeat number that is important during homologous
719 recombination. *Mol Microbiol* **68**, 1237-1251, doi:10.1111/j.1365-2958.2008.06230.x (2008).

720 31 Devlin, R. *et al.* Mapping replication dynamics in *Trypanosoma brucei* reveals a link with
721 telomere transcription and antigenic variation. *Elife* **5**, doi:10.7554/eLife.12765 (2016).

722 32 Kim, H. S. & Cross, G. A. TOPO3alpha influences antigenic variation by monitoring
723 expression-site-associated VSG switching in *Trypanosoma brucei*. *PLoS Pathog* **6**, e1000992,
724 doi:10.1371/journal.ppat.1000992 (2010).

725 33 Kim, H. S. & Cross, G. A. Identification of *Trypanosoma brucei* RMI1/BLAP75 homologue and
726 its roles in antigenic variation. *PLoS One* **6**, e25313, doi:10.1371/journal.pone.0025313
727 (2011).

728 34 Black, J. A. *et al.* *Trypanosoma brucei* ATR Links DNA Damage Signaling during Antigenic
729 Variation with Regulation of RNA Polymerase I-Transcribed Surface Antigens. *Cell Rep* **30**,
730 836-851 e835, doi:10.1016/j.celrep.2019.12.049 (2020).

731 35 Glover, L. & Horn, D. Locus-specific control of DNA resection and suppression of subtelomeric
732 VSG recombination by HAT3 in the African trypanosome. *Nucleic Acids Res* **42**, 12600-
733 12613, doi:10.1093/nar/gku900 (2014).

734 36 Ciccio, A. & Elledge, S. J. The DNA damage response: making it safe to play with knives. *Mol*
735 *Cell* **40**, 179-204, doi:10.1016/j.molcel.2010.09.019 (2010).

736 37 Syed, A. & Tainer, J. A. The MRE11-RAD50-NBS1 Complex Conducts the Orchestration of
737 Damage Signaling and Outcomes to Stress in DNA Replication and Repair. *Annu Rev*
738 *Biochem* **87**, 263-294, doi:10.1146/annurev-biochem-062917-012415 (2018).

739 38 Lisby, M., Barlow, J. H., Burgess, R. C. & Rothstein, R. Choreography of the DNA damage
740 response: spatiotemporal relationships among checkpoint and repair proteins. *Cell* **118**, 699-
741 713, doi:10.1016/j.cell.2004.08.015 (2004).

742 39 Myler, L. R. *et al.* Single-Molecule Imaging Reveals How Mre11-Rad50-Nbs1 Initiates DNA
743 Break Repair. *Mol Cell* **67**, 891-898 e894, doi:10.1016/j.molcel.2017.08.002 (2017).

744 40 Paull, T. T. & Gellert, M. The 3' to 5' exonuclease activity of Mre 11 facilitates repair of DNA
745 double-strand breaks. *Mol Cell* **1**, 969-979 (1998).

746 41 Zhang, Y., Zhou, J. & Lim, C. U. The role of NBS1 in DNA double strand break repair,
747 telomere stability, and cell cycle checkpoint control. *Cell Res* **16**, 45-54,
748 doi:10.1038/sj.cr.7310007 (2006).

749 42 Paudyal, S. C. & You, Z. Sharpening the ends for repair: mechanisms and regulation of DNA
750 resection. *Acta Biochim Biophys Sin (Shanghai)* **48**, 647-657, doi:10.1093/abbs/gmw043
751 (2016).

752 43 Hopfner, K. P. *et al.* Structural biology of Rad50 ATPase: ATP-driven conformational control in
753 DNA double-strand break repair and the ABC-ATPase superfamily. *Cell* **101**, 789-800,
754 doi:10.1016/s0092-8674(00)80890-9 (2000).

755 44 Oh, J. & Symington, L. S. Role of the Mre11 Complex in Preserving Genome Integrity. *Genes*
756 (*Basel*) **9**, doi:10.3390/genes9120589 (2018).

757 45 Longhese, M. P. DNA damage response at functional and dysfunctional telomeres. *Genes*
758 *Dev* **22**, 125-140, doi:10.1101/gad.1626908 (2008).

759 46 Robinson, N. P., McCulloch, R., Conway, C., Browitt, A. & Barry, J. D. Inactivation of Mre11
760 does not affect VSG gene duplication mediated by homologous recombination in
761 *Trypanosoma brucei*. *J Biol Chem* **277**, 26185-26193, doi:10.1074/jbc.M203205200 (2002).

762 47 Tan, K. S., Leal, S. T. & Cross, G. A. *Trypanosoma brucei* MRE11 is non-essential but
763 influences growth, homologous recombination and DNA double-strand break repair. *Mol*
764 *Biochem Parasitol* **125**, 11-21 (2002).

765 48 Hopfner, K. P. *et al.* Structural biochemistry and interaction architecture of the DNA double-
766 strand break repair Mre11 nuclease and Rad50-ATPase. *Cell* **105**, 473-485 (2001).

767 49 Laffitte, M. C. *et al.* Chromosomal Translocations in the Parasite *Leishmania* by a
768 MRE11/RAD50-Independent Microhomology-Mediated End Joining Mechanism. *PLoS Genet*
769 **12**, e1006117, doi:10.1371/journal.pgen.1006117 (2016).

770 50 Hopfner, K. P. *et al.* The Rad50 zinc-hook is a structure joining Mre11 complexes in DNA
771 recombination and repair. *Nature* **418**, 562-566, doi:10.1038/nature00922 (2002).

772 51 Williams, R. S., Williams, J. S. & Tainer, J. A. Mre11-Rad50-Nbs1 is a keystone complex
773 connecting DNA repair machinery, double-strand break signaling, and the chromatin template.
774 *Biochem Cell Biol* **85**, 509-520, doi:10.1139/O07-069 (2007).

775 52 De la Rosa, M. B. & Nelson, S. W. An interaction between the Walker A and D-loop motifs is
776 critical to ATP hydrolysis and cooperativity in bacteriophage T4 Rad50. *J Biol Chem* **286**,
777 26258-26266, doi:10.1074/jbc.M111.256305 (2011).

778 53 Kelley, L. A., Mezulis, S., Yates, C. M., Wass, M. N. & Sternberg, M. J. The Phyre2 web portal
779 for protein modeling, prediction and analysis. *Nat Protoc* **10**, 845-858,
780 doi:10.1038/nprot.2015.053 (2015).

781 54 Jackson, S. P. & Bartek, J. The DNA-damage response in human biology and disease. *Nature*
782 **461**, 1071-1078, doi:10.1038/nature08467 (2009).

783 55 Glover, L. & Horn, D. Trypanosomal histone gammaH2A and the DNA damage response. *Mol*
784 *Biochem Parasitol* **183**, 78-83, doi:10.1016/j.molbiopara.2012.01.008 (2012).

785 56 Stauffer, M. E. & Chazin, W. J. Physical interaction between replication protein A and Rad51
786 promotes exchange on single-stranded DNA. *J Biol Chem* **279**, 25638-25645,
787 doi:10.1074/jbc.M400029200 (2004).

788 57 Ingram, A. K., Cross, G. A. & Horn, D. Genetic manipulation indicates that ARD1 is an
789 essential N(alpha)-acetyltransferase in *Trypanosoma brucei*. *Mol Biochem Parasitol* **111**, 309-
790 317 (2000).

791 58 Glover, L. *et al.* Antigenic variation in African trypanosomes: the importance of chromosomal
792 and nuclear context in VSG expression control. *Cell Microbiol* **15**, 1984-1993,
793 doi:10.1111/cmi.12215 (2013).

794 59 Stockdale, C., Swiderski, M. R., Barry, J. D. & McCulloch, R. Antigenic variation in
795 *Trypanosoma brucei*: joining the DOTs. *PLoS Biol* **6**, e185, doi:10.1371/journal.pbio.0060185
796 (2008).

797 60 Connelly, J. C. & Leach, D. R. Tethering on the brink: the evolutionarily conserved Mre11-
798 Rad50 complex. *Trends Biochem Sci* **27**, 410-418 (2002).

799 61 Rico, E., Jeacock, L., Kovarova, J. & Horn, D. Inducible high-efficiency CRISPR-Cas9-
800 targeted gene editing and precision base editing in African trypanosomes. *Sci Rep* **8**, 7960,
801 doi:10.1038/s41598-018-26303-w (2018).

802 62 Waldrip, Z. J. *et al.* A CRISPR-based approach for proteomic analysis of a single genomic
803 locus. *Epigenetics* **9**, 1207-1211, doi:10.4161/epi.29919 (2014).

804 63 Zhang, W. W. & Matlashewski, G. CRISPR-Cas9-Mediated Genome Editing in *Leishmania*
805 *donovani*. *MBio* **6**, doi:10.1128/mBio.00861-15 (2015).

806 64 Grenon, M., Gilbert, C. & Lowndes, N. F. Checkpoint activation in response to double-strand
807 breaks requires the Mre11/Rad50/Xrs2 complex. *Nat Cell Biol* **3**, 844-847,
808 doi:10.1038/ncb0901-844 (2001).

809 65 Marechal, A. & Zou, L. DNA damage sensing by the ATM and ATR kinases. *Cold Spring Harb*
810 *Perspect Biol* **5**, doi:10.1101/cshperspect.a012716 (2013).

811 66 Laffitte, M. C. *et al.* Formation of linear amplicons with inverted duplications in *Leishmania*
812 requires the MRE11 nuclease. *PLoS Genet* **10**, e1004805, doi:10.1371/journal.pgen.1004805
813 (2014).

814 67 Gomes Passos Silva, D. *et al.* The in vivo and in vitro roles of *Trypanosoma cruzi* Rad51 in
815 the repair of DNA double strand breaks and oxidative lesions. *PLoS Negl Trop Dis* **12**,
816 e0006875, doi:10.1371/journal.pntd.0006875 (2018).

817 68 Westmoreland, J. *et al.* RAD50 is required for efficient initiation of resection and
818 recombinational repair at random, gamma-induced double-strand break ends. *PLoS Genet* **5**,
819 e1000656, doi:10.1371/journal.pgen.1000656 (2009).

820 69 Zhu, Z., Chung, W. H., Shim, E. Y., Lee, S. E. & Ira, G. Sgs1 helicase and two nucleases
821 Dna2 and Exo1 resect DNA double-strand break ends. *Cell* **134**, 981-994,
822 doi:10.1016/j.cell.2008.08.037 (2008).

823 70 Seol, J. H., Shim, E. Y. & Lee, S. E. Microhomology-mediated end joining: Good, bad and
824 ugly. *Mutat Res* **809**, 81-87, doi:10.1016/j.mrfmmm.2017.07.002 (2018).

825 71 Barnes, R. L. & McCulloch, R. *Trypanosoma brucei* homologous recombination is dependent
826 on substrate length and homology, though displays a differential dependence on mismatch

827 repair as substrate length decreases. *Nucleic Acids Res* **35**, 3478-3493,
828 doi:10.1093/nar/gkm249 (2007).

829 72 Briggs, E., Crouch, K., Lemgruber, L., Lapsley, C. & McCulloch, R. Ribonuclease H1-targeted
830 R-loops in surface antigen gene expression sites can direct trypanosome immune evasion.
831 *PLoS Genet* **14**, e1007729, doi:10.1371/journal.pgen.1007729 (2018).

832 73 Briggs, E. *et al.* Trypanosoma brucei ribonuclease H2A is an essential R-loop processing
833 enzyme whose loss causes DNA damage during transcription initiation and antigenic
834 variation. *Nucleic Acids Res*, doi:10.1093/nar/gkz644 (2019).

835 74 Chang, E. Y. *et al.* MRE11-RAD50-NBS1 promotes Fanconi Anemia R-loop suppression at
836 transcription-replication conflicts. *Nat Commun* **10**, 4265, doi:10.1038/s41467-019-12271-w
837 (2019).

838 75 Balestrini, A. *et al.* Defining ATM-Independent Functions of the Mre11 Complex with a Novel
839 Mouse Model. *Mol Cancer Res* **14**, 185-195, doi:10.1158/1541-7786.MCR-15-0281 (2016).

840 76 Schlacher, K. *et al.* Double-strand break repair-independent role for BRCA2 in blocking stalled
841 replication fork degradation by MRE11. *Cell* **145**, 529-542, doi:10.1016/j.cell.2011.03.041
842 (2011).

843 77 Jehi, S. E., Nanavaty, V. & Li, B. Trypanosoma brucei TIF2 and TRF Suppress VSG Switching
844 Using Overlapping and Independent Mechanisms. *PLoS One* **11**, e0156746,
845 doi:10.1371/journal.pone.0156746 (2016).

846 78 Ira, G. & Haber, J. E. Characterization of RAD51-independent break-induced replication that
847 acts preferentially with short homologous sequences. *Mol Cell Biol* **22**, 6384-6392,
848 doi:10.1128/mcb.22.18.6384-6392.2002 (2002).

849 79 Hirumi, H. & Hirumi, K. Continuous cultivation of Trypanosoma brucei blood stream forms in a
850 medium containing a low concentration of serum protein without feeder cell layers. *J Parasitol*
851 **75**, 985-989 (1989).

852 80 van den Hoff, M. J., Moorman, A. F. & Lamers, W. H. Electroporation in 'intracellular' buffer
853 increases cell survival. *Nucleic Acids Res* **20**, 2902 (1992).

854 81 Jeacock, L., Baker, N., Wiedemar, N., Maser, P. & Horn, D. Aquaglyceroporin-null
855 trypanosomes display glycerol transport defects and respiratory-inhibitor sensitivity. *PLoS*
856 *Pathog* **13**, e1006307, doi:10.1371/journal.ppat.1006307 (2017).

857 82 Alsford, S. & Horn, D. Single-locus targeting constructs for reliable regulated RNAi and
858 transgene expression in Trypanosoma brucei. *Mol Biochem Parasitol* **161**, 76-79,
859 doi:10.1016/j.molbiopara.2008.05.006 (2008).

860 83 Alsford, S. & Horn, D. Single-locus targeting constructs for reliable regulated RNAi and
861 transgene expression in *Trypanosoma brucei*. *Mol Biochem Parasitol* **161**, 76-79,
862 doi:10.1016/j.molbiopara.2008.05.006 (2008).

863 84 Devlin, R. *et al.* Mapping replication dynamics in Trypanosoma brucei reveals a link with
864 telomere transcription and antigenic variation. *eLife* **5**, e12765, doi:10.7554/eLife.12765
865 (2016).

- 866 85 Gong, F. & Miller, K. M. Mammalian DNA repair: HATs and HDACs make their mark through
867 histone acetylation. *Mutation research* **750**, 23-30, doi:10.1016/j.mrfmmm.2013.07.002 (2013).
- 868 86 Woodward, R. & Gull, K. Timing of nuclear and kinetoplast DNA replication and early
869 morphological events in the cell cycle of *Trypanosoma brucei*. *J Cell Sci* **95 (Pt 1)**, 49-57
870 (1990).
- 871 87 Langmead, B. & Salzberg, S. L. Fast gapped-read alignment with Bowtie 2. *Nat Methods* **9**,
872 357-359, doi:10.1038/nmeth.1923 (2012).
- 873 88 Li, H. *et al.* The Sequence Alignment/Map format and SAMtools. *Bioinformatics* **25**, 2078-
874 2079, doi:10.1093/bioinformatics/btp352 (2009).
- 875 89 Liao, Y., Smyth, G. K. & Shi, W. featureCounts: an efficient general purpose program for
876 assigning sequence reads to genomic features. *Bioinformatics* **30**, 923-930,
877 doi:10.1093/bioinformatics/btt656 (2014).
- 878 90 Robinson, M. D., McCarthy, D. J. & Smyth, G. K. edgeR: a Bioconductor package for
879 differential expression analysis of digital gene expression data. *Bioinformatics* **26**, 139-140,
880 doi:10.1093/bioinformatics/btp616 (2010).

881

882

883 **TABLE AND SUPPLEMENTARY FIGURE LEGENDS**

884

885 **Supplementary figure 1:** Sequence alignment of the *T. brucei* RAD50 (*TbRAD50*) with *Homo*
886 *sapiens* (*HsRAD50*; UNIPROT: Q92878). Conserved domains are highlighted in bold and the
887 ABC/ATPase domains highlighted with grey bar. Highly conserved residues are highlighted with a *
888 and residues with conserved properties with ':' or '!'.

889

890 **Supplementary figure 2:** Generation of *rad50* and *mre11* null strains. (A) Upper panel: Schematic
891 showing the knockout strategy to generate the chromosome-internal ¹HR*rad50* null cell line. (B) PCR
892 assay confirming *RAD50* double allele replacement. (C) PCR assay confirming *MRE11* double allele
893 replacement. * background band. *NEO*, Neomycin Phosphotransferase; *BLA*, Blasticidin deaminase.
894 C1, control plasmid for *BLA*; C2, control plasmid for *NEO*.

895

896 **Supplementary figure 3:** Resection is compromised in the ¹HR*rad50* nulls Left panel: Biological
897 replicate showing accumulation of ssDNA was monitored using slot-blots, n=2 for biological replicates.
898 Right panel: Quantitative analysis the amount of ssDNA. Error bars, SD for biological replicates for the
899 *rad50* null strains; n=2.

900

901 **Supplementary figure 4:** MRE11 is essential for DSB response and repair at a chromosome-internal
902 locus. (A) Clonogenic assay reveals survivors following a DSB at a chromosome-internal locus in the
903 parental and ¹HR*mre11* null cell lines. Details as in Figure 1 ¹HR technical replicates; n=2, and with
904 ¹HR*mre11* biological replicates for the strains; n=2. (B) Upper panel: Immunofluorescence assay to
905 monitoring γ H2A foci. The number of positive nuclei were counted in uninduced cells and 12 hours

906 post DSB. Middle panel: Immunofluorescence assay to monitoring RAD51 foci. The number of positive
907 nuclei were counted in uninduced cells and 12 hours post DSB. Lower panel: The number of cells in
908 G2/M phase cells was counted by DAPI staining at several points following induction of an I-SceI
909 break in. G2 cells contain one nucleus and two kinetoplasts. Error bars, SD, for ¹HR*mre11* biological
910 replicates for the strains; n=2. (C) PCR analysis of repaired subclones. Upper panel: Schematic
911 showing the 2110 locus and position of the *Sce* recognition site (*Sce*^R). Position of primers indicated
912 by arrows. Primer sequence detailed in materials and methods. Middle panel: PCR assay of repaired
913 subclones showing *RFP:PAC* presence or absence. Lower panel: PCR assay of repaired subclones
914 that were negative for *RFP:PAC*. Arrows indicate position of primers. White box, genes; Grey box,
915 *RFP:PAC* fusion gene; black box, UTRs.

916

917 **Supplementary figure 5:** Analysis of VSG^{up}*RAD50* strains. (A) Schematic showing the telomeric end
918 of the VSG2 BES. (B) Presence or absence of *ESAG1* in the repaired subclones. (C) Presence or
919 absence of VSG2 in the repaired subclones. Arrows indicate position of primers; box with diagonal
920 lines, 70-bp repeats; white boxes, genes; ψ , VSG pseudo gene; vertical lines, telomere.

921

922 **Supplementary figure 6:** MRE11 is essential for DSB response and repair at an expression site. (A)
923 Clonogenic assay reveals survivors following a DSB in the VSG^{up} strain in the parental and
924 VSG^{up}*mre11* cell lines. Details as in Figure 1 (B) Upper panel: Immunofluorescence assay to
925 monitoring γ H2A foci. The number of positive nuclei were counted in uninduced cells and 12 hours
926 post DSB. Lower panel: The number of cells in G2/M phase cells was counted by DAPI staining at
927 several points following induction of an I-SceI break in. G2 cells contain one nucleus and two
928 kinetoplasts. Error bars, SD, for VSG^{up}*mre11* biological replicates for the strains; n=2. (C) PCR
929 analysis of repaired subclones. Upper panel: Schematic showing BES1. Position of primers indicated
930 by arrows. Primer sequence detailed in materials and methods. Middle panel: PCR assay of repaired
931 subclones showing *ESAG1* presence or absence. Lower panel: PCR assay of repaired subclones that
932 were negative for VSG2 by immunofluorescence. Arrows indicate position of primers. White box,
933 genes; ψ , pseudo gene; lined box, 70 bp repeats; black box, UTRs. VSG^{up}*mre11* biological
934 replicates for the strains; n=2.

935

936

937 **Supplementary figure 7:** (A) Table showing position of the VSG genes used for recombination (C)
938 Proportion of VSG2 in the populations before and after induction of a DSB. (D) Schematic represents
939 the telomeric end of the VSG2 ES. BLAST analysis of significantly up-regulated genes. BLAST hits
940 are represented as lines showing their position on the VSG2 query sequence. Black lines – VSG
941 genes significantly enriched in both VSG^{up} and VSG^{up}*rad50*, blue bars – VSG^{up} only, red bars –
942 VSG^{up}*rad50* only.

943

944 **Table 1:** Details of clonogenic assays of strains described in this manuscript following a DSB.

945

Supplementary Figure 1

Walker A/P-loop

HsRAD50	MSRIEKMSILGVRSGIEDKDKQIITFFSPLTILV GPNGAGKT TIIIECLKYICTGDFPPG	60
TbRAD50	MTSIEQIEISGVRSDPNPNRQRIIVFKKPLTVILGKNGAGKTTIEALLNACTGQMPPG	60
	*: **: :.* *****. : : : * *. * .***: : * *****.* ****: :***	
	ABC RAD50 N	

HsRAD50	T--KGNTFVHDPKVAQETDVRAQIRLQFRDVGELIIVQSRSMVCTQKSKKTEFKTLEGVI	118
TbRAD50	GGTEKSSFVYDPKVVGENDVKAQIRLLFTGRGGKVMQVIRSFQATRTRNKTFATLDNIV	120
	: .:***:****. *.**:* ***** * . .*: : : * ** : .*: . : ** * ** : : :	

Q-loop/lid

HsRAD50	TRT--KHGEKVSLSKCAEIDREMISLGVSKAVLNNV IFCH QEDSNWPLSEGKALKQKF	176
TbRAD50	AFQDSATGKIISSTYRANDVDRAIPDMLGVS PAVLEHVI FCHQEDGNWPLSPKVEKKIF	180
	: * : * : : . : : * : . **** * : : * : * : * : * : * : * : * : * : *	

MRE11 binding site

HsRAD50	DEIFSATRYIKALETLRQVRQTQGG KVKEYQMEKYLKQYKEKACEIRDQITSKEAQLTS	236
TbRAD50	DDIFAATRYVLALDRLRENNKELRRQQKEHEASLMSLSEHREQARQISADITVKEETVAG	240
	*.**:****: **: **: . : : : : : : . * * . : : : * : * : * * ** : : .	

Zn hook

HsRAD50	IEKSSKQRAMLAGAT--AVYSQFITQLTDENQSC CPVC QRVFQTEAELQEVISDLQSKL	705
TbRAD50	RDRYHKLNEKLSGSKALAACHAHFVEQ--AKVEDKCPLCGRAFSGENELNDFLASFKVGG	714
	: : * . * : * . * : : * : * : : . ** : * * . * : * * : : : : : :	

HsRAD50	KLEENIDNIKRHNHLALGRQKGYEEEEIHFKKELREPQFRDAEEKYREMMIVMRTTEL VN	1118
TbRAD50	LIRGKISALECLRAQQDGVAEAMRQDIESLKGQLTRDKYKDIEKRYRTTFLKVQTTEIAV	1159
	: . : * . : : : * : . . : : * : * : * . : : : * * : * : * : : : * : * : :	

MRE11 binding site

HsRAD50	KDLDIYYKTLDAQAIMKFHSMKME EINKIIRDLRSTYRGQDIEYIEIRSDADENVSASDK	1178
TbRAD50	SDVEKYRALEKAVQTYHQEKIAQINQILADLRHTYKGSIDITIELRSEDD--VTSTTA	1217
	. * : : * : * : * : * : . : * . * : : * : * : * * * * : * : * : * : * : :	

ABC transporter signature motif

Walker B D-loop

HsRAD50	RRNYNYRVVMLKGDALDMRGR CSAGQKVLAS LIIRLALAEFCLNCG IIALDEPTTNLD	1238
TbRAD50	RRSYSYRVVMKRGNSMDMRGRCSAGQKVLASVLIIRLALAEAFCCDCGILALDEPTTNLD	1277
	** . * . ***** : * : : : ***** : ***** : * : * : * : * : * : * : *	

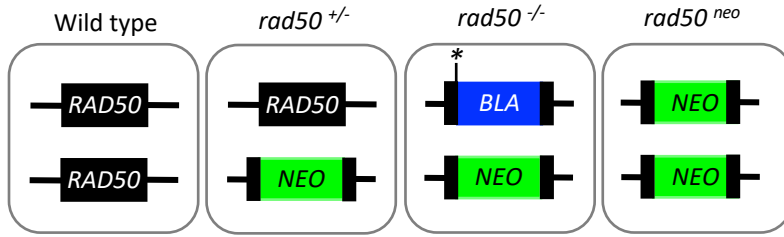
H-loop/switch region

HsRAD50	RENIESLAHALVEI IKRSRQQRNFQL LVI THDE DFVELLGRSEYVEKFYRIKKNIDQCSE	1298
TbRAD50	EDNARSLAESLRMLIDSHRAVKHFQLIVITHDEHFVRALGGQALDT-FYYIHKDREGAFS	1336
	. : * . *** : : * : * : : : * : * : * * * * . ** * : * : : . . .	
	ABC RAD50 C	

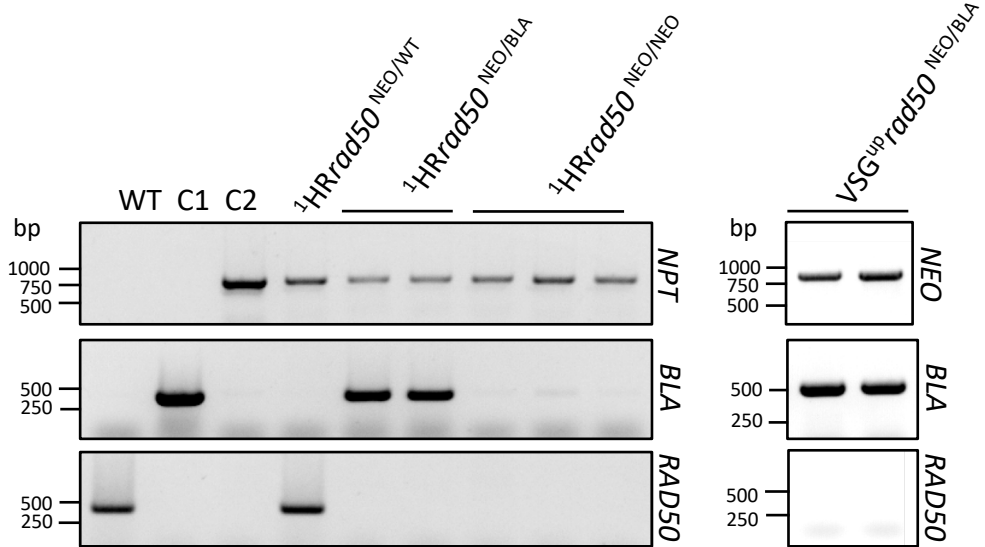
HsRAD50	IVKCSVSSLGFNVH	1312
TbRAD50	VIEERTFDQLFAS-	1349
	: : : . . *	

Supplementary Figure 2

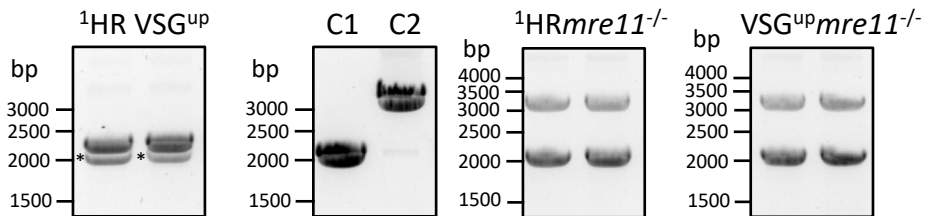
A



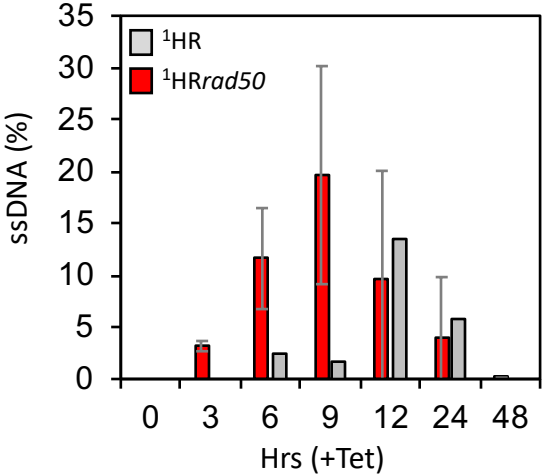
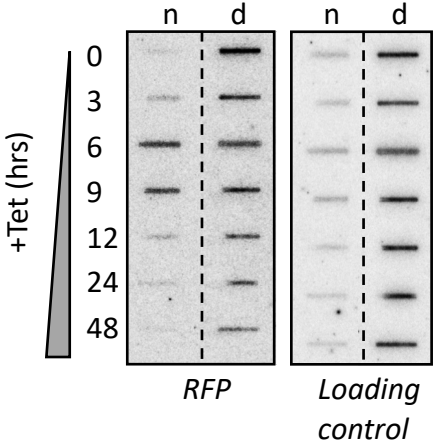
B



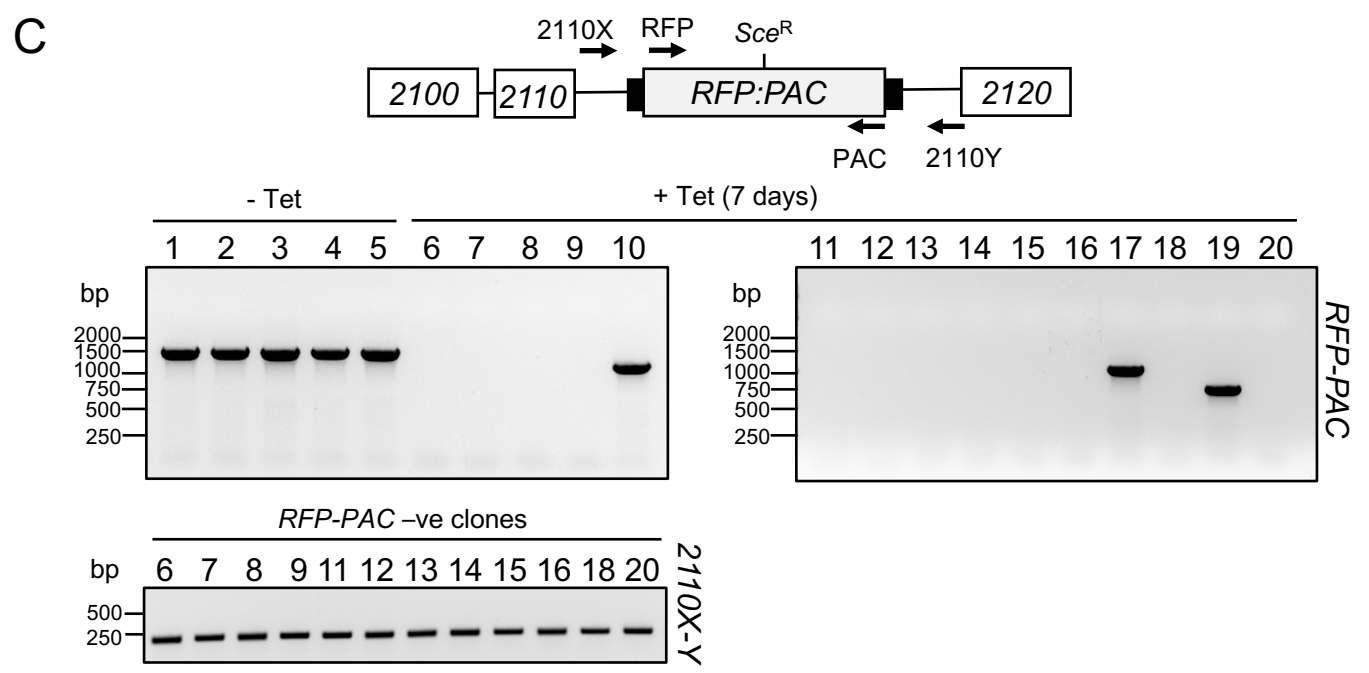
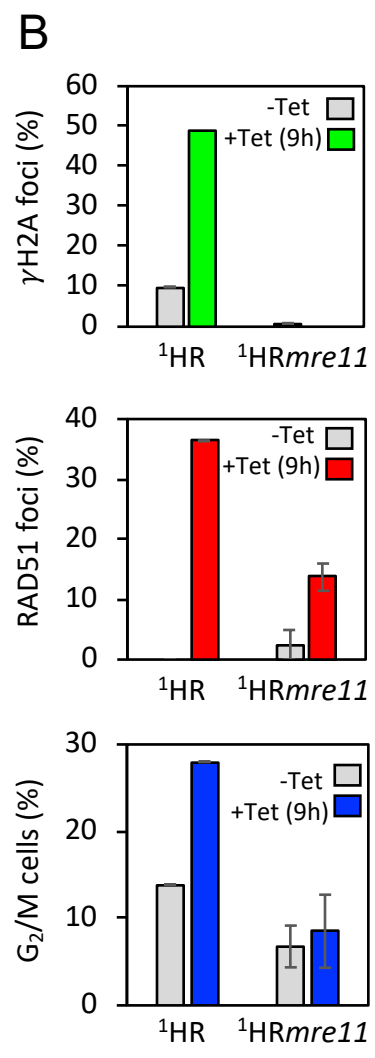
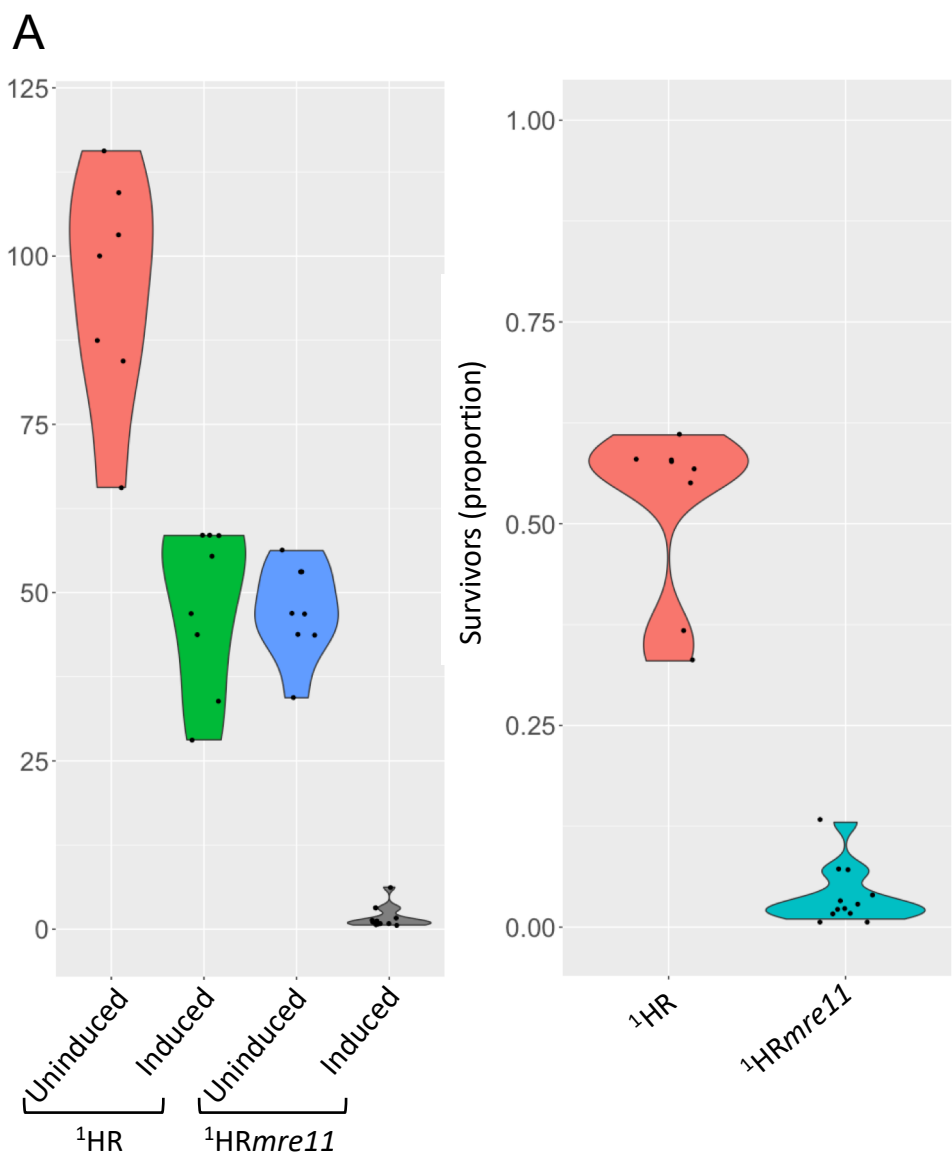
C



Supplementary Figure 3

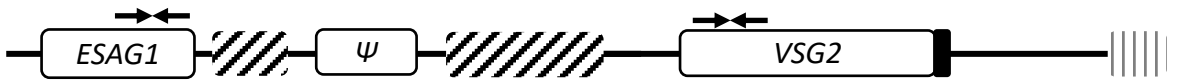


Supplementary Figure 4

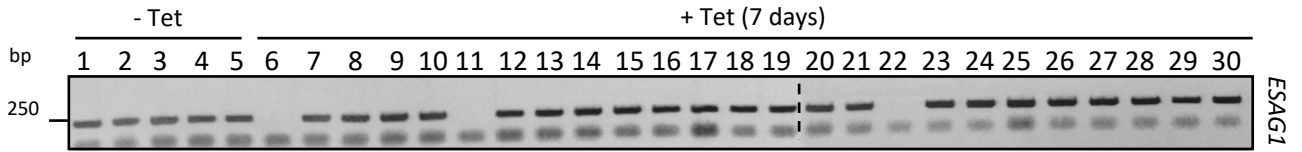


Supplementary Figure 5

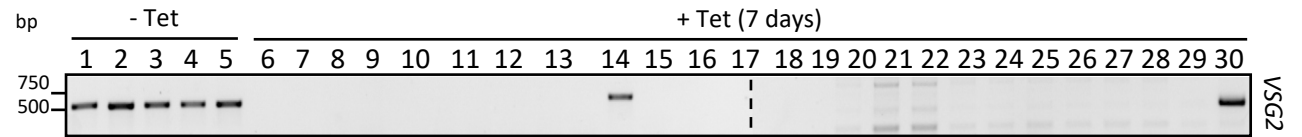
A



B

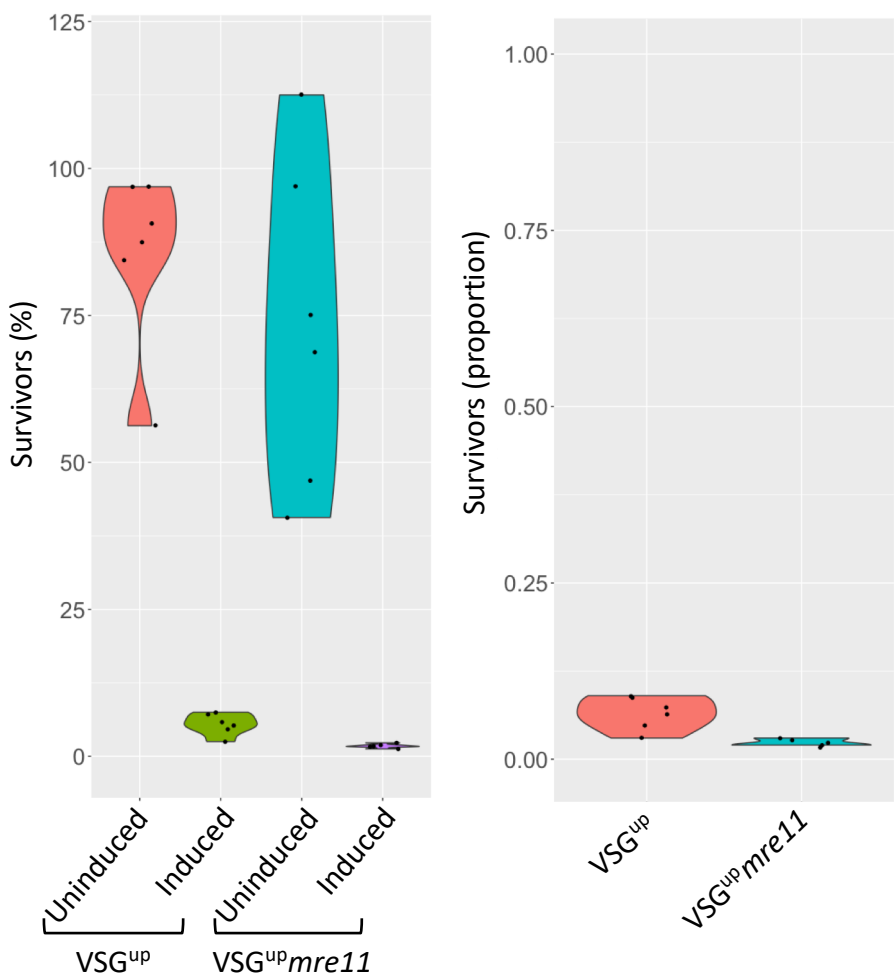


C

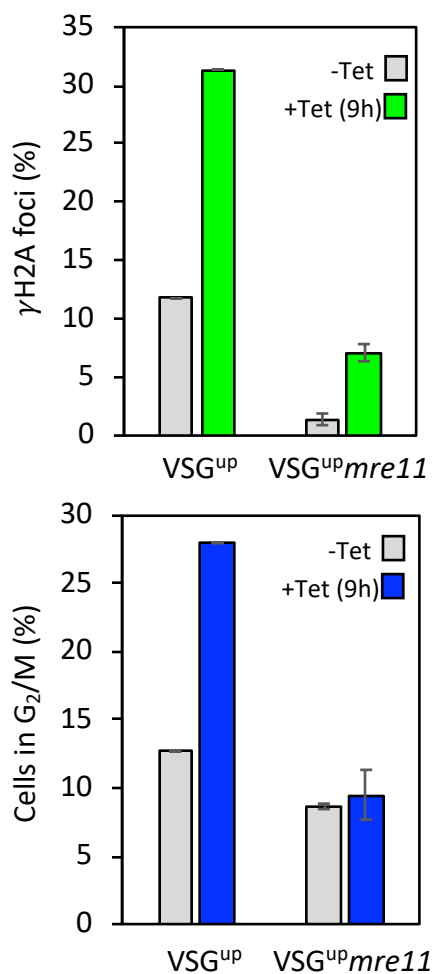


Supplementary Figure 6

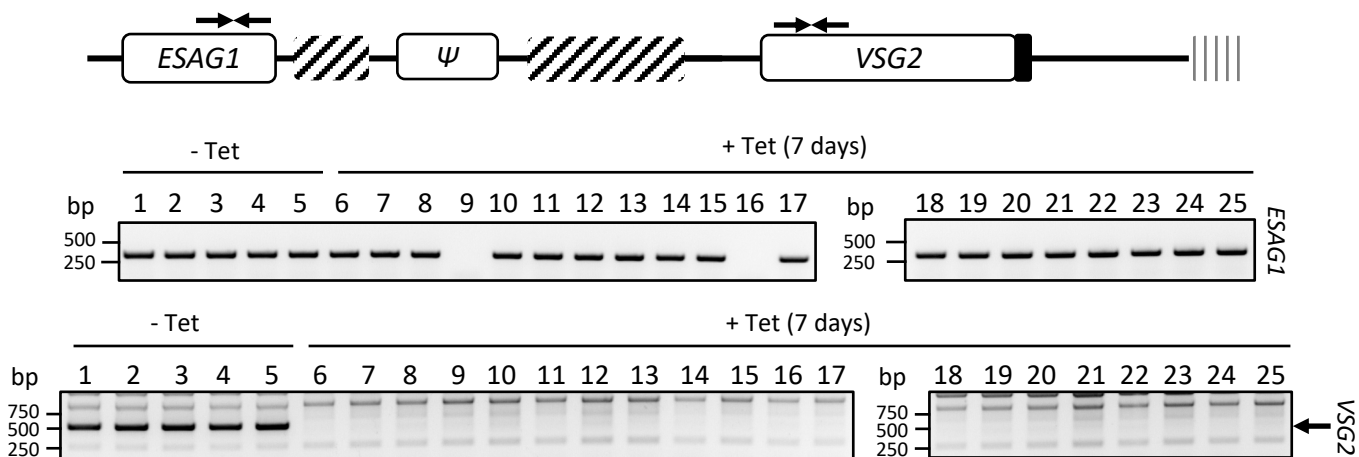
A



B



C



Supplementary Figure 7

A

	VSG ^{up}	VSG ^{up} <i>rad50</i>
Total	83	225
BES	10	11
Minichromosome	22	30
Megabase	29	150
Other	22	34

B

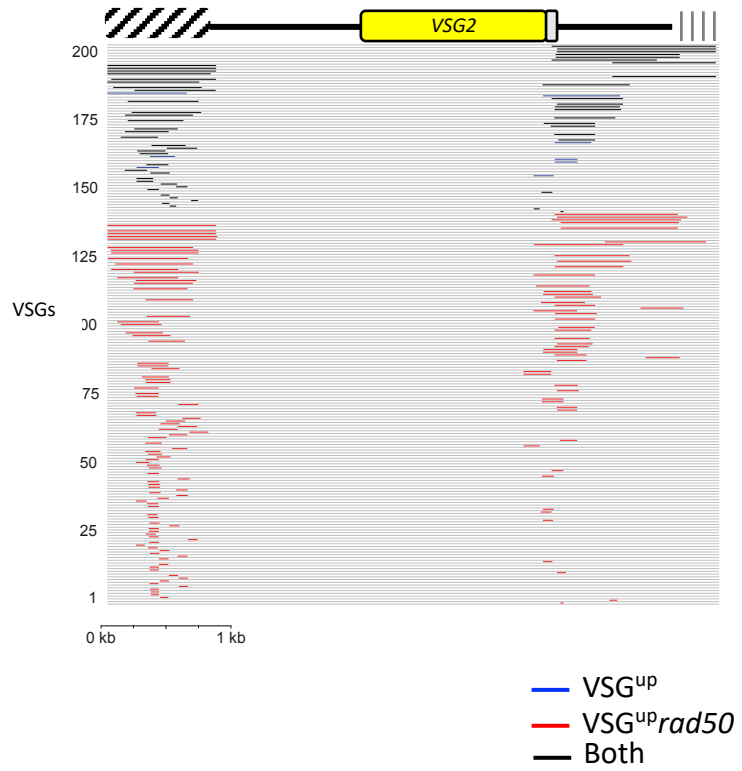


Table 1

Strain	Uninduced (%)	SD	Induced (%)	SD	Proportion	SD
¹ HR	95.09	+/- 17.1	47.9	+/-11.93	0.52	+/- 0.1
¹ HR <i>rad50</i>	35.76	+/- 6.83	2.91	+/- 4.36	0.08	+/- 0.12
¹ HR <i>mre11</i>	47.27	+/- 6.97	1.79	+/- 1.65	0.04	+/- 0.03
VSG ^{up}	85.42	+/- 15.1	5.45	+/- 1.81	0.07	+/- 0.02
VSG ^{up} <i>rad50</i>	51.04	+/- 16.3	5.81	+/- 1.64	0.11	+/- 0.03
VSG ^{up} <i>mre11</i>	73.44	+/- 27.86	1.75	+/- 0.37	0.02	+/- 0.005